

The Impact of Fc γ RI Binding on ImmunoPET

*Delphine Vivier^{1,†}, Sai Kiran Sharma^{2,†}, Pierre Adumeau¹, Cindy Rodriguez¹, Kimberly Fung^{1,3},
Brian M. Zeglis^{1,2,3*}*

¹Department of Chemistry, Hunter College of the City University of New York, New York, NY 10021,
United States

²Department of Radiology, Memorial Sloan Kettering Cancer Center, New York, NY 10065, United
States

³Ph.D. Program in Chemistry, The Graduate Center of the City University of New York, New York, NY,
10016, United States

[†]These two authors contributed equally to this work.

First Authors: Delphine Vivier: Université de Bourgogne, 9 Avenue Alain Savary, Dijon, France, E-mail: delphine.vivier@u-bourgogne.fr. Sai Kiran Sharma: Memorial Sloan Kettering Cancer Center, 1275 York Avenue, New York, NY, E-mail: sharmas@mskcc.org.

Corresponding Author: Brian M. Zeglis. 413 East 69th Street, New York, NY, 10021. Phone: 212-896-0433. E-mail: bz102@hunter.cuny.edu.

Word Count (including references): 5,991

Running Title: Fc γ RI Binding and ImmunoPET

Keywords: Glycans, Fc region, Fc receptor, Fc γ RI, PET, radioimmunoconjugate

Disclosure Statement: No potential conflicts of interest relevant to this article exist.

ABSTRACT

Antibodies are promising vectors for positron-emission tomography (PET) imaging. However, the high uptake of radioimmunoconjugates in non-target tissues such as the liver and spleen hampers their performance as radiotracers. This off-target uptake can lead to suboptimal tumor-to-background activity concentration ratios, decreasing the contrast of images and reducing their diagnostic utility. A possible cause of this uptake is the sequestration of radioimmunoconjugates by immune cells bearing Fc-gamma receptors (Fc γ R) that bind to the Fc regions of antibodies.

Methods: Since the heavy chain glycans influence the affinity of Fc γ R for the Fc domain, we set out to investigate whether radioimmunoconjugates with truncated glycans would exhibit altered binding to Fc γ RI and, in turn, improved *in vivo* performance. Using the HER2-targeting antibody trastuzumab, we synthesized a series of desferrioxamine (DFO)-bearing immunoconjugates with differing glycosylation states and interrogated their Fc γ RI binding via surface plasmon resonance (SPR), ELISA, and flow cytometry. Furthermore, we labeled these immunoconjugates with ^{89}Zr and explored their biodistribution in athymic nude, NSG, and humanized NSG mice bearing HER2-expressing human breast cancer xenografts.

Results: We observed a strong correlation between the impaired *in vitro* Fc γ RI binding of deglycosylated immunoconjugates and significant decreases in the *in vivo* off-target uptake of the corresponding ^{89}Zr -labeled radioimmunoconjugates (*i.e.* liver activity concentrations are reduced by ~3.5-fold in humanized NSG mice). These reductions in off-target uptake were accompanied by concomitant increases in the tumoral activity concentrations of the glycoengineered radioimmunoconjugates, ultimately yielding improved tumor-to-healthy organ contrast and higher quality PET images.

Conclusions: Our findings suggest that the deglycosylation of antibodies represents a facile strategy for improving the quality of immunoPET in animal models as well as in certain patient populations.

INTRODUCTION

Over the past two decades, antibody-based positron emission tomography (immunoPET) has emerged as a clinically relevant technology for the staging, treatment planning, and treatment monitoring of cancer (1). Not surprisingly, however, immunoPET has its drawbacks. For example, the sluggish *in vivo* pharmacokinetics of antibodies means that sufficient image contrast can only be obtained >72 h after the administration of the tracer. Furthermore, the high molecular weight (~150 kDa) of full-length antibodies directs their clearance to the hepatobiliary system, often resulting in the accumulation of radioactivity in the healthy liver and spleen. A less well-described phenomenon that contributes to the non-specific uptake of antibodies is their inherent ability to interact with the immune system. While the Fab portion of an antibody is responsible for binding to antigens, the Fc region engages in interactions with Fc receptors, most notably Fc-gamma receptors (Fc γ R) and the neonatal Fc receptor (FcRn) (Fig. 1A). The binding of the latter facilitates the antibody's escape from lysosomal degradation, which in turn leads to its *in vivo* recycling and extended serum half-life. In contrast, the interactions between Fc γ R expressed on immune effector cells and the Fc region of antibodies can trigger antibody-mediated therapeutic responses (2,3). Critically, the affinity of Fc γ R is sensitive to the glycosylation state of the antibody, while that of FcRn is not (4). Although interactions with Fc γ R are critical for therapeutic antibodies, they may not be favorable in the context of molecular imaging (5). Indeed, the immune response sparked by the binding of antibodies to Fc γ R may lead to the sequestration of radioimmunoconjugates in healthy non-target tissues, decreasing tumor-to-background contrast and dampening the quality and diagnostic utility of the images.

Several approaches to circumventing this issue have been proposed. For example, a great deal of attention has been dedicated to antibody fragments such as Fab and F(ab)₂, which not only have more rapid pharmacokinetic profiles compared to full-length antibodies but also lack the Fc region responsible for interactions with the immune system. However, these traits undoubtedly come at a price: very high activity concentrations in the kidneys and tumoral activity concentrations that are only a fraction of those obtained using intact immunoglobulin G (IgGs) (6). Another strategy is predicated on genetically engineering the Fc region of an IgG to abrogate its binding with Fc γ Rs on immune cells while maintaining its ability to bind FcRn (7).

This method is effective, yet it is complex, expensive, and requires specialized genetic engineering.

A more facile and modular approach may lie in manipulating the glycans of the Fc region. In recent years, the role of the Fc region in the *in vivo* behavior of antibodies has been the subject of increasing attention, and the role of glycosylation in the binding of IgG1 to Fc γ R has become a focal point (8). Indeed, IgGs contain a conserved *N*-linked glycosylation site — Asn-X-Ser/Thr, where X can be any amino acid except proline — within the C_{H2} domain of each heavy chain of the Fc region (9,10). The *N*-linked complex glycan attached to each Asn297 is a bi-antennary heptasaccharide chain composed of *N*-acetylglucosamine and mannose residues that can be decorated with fucose, galactose, and sialic acid (Fig. 1A). While the glycans are not directly involved in the antibody's interaction with Fc γ R, several studies have shown that these sugar chains control the 3-dimensional configuration of the Fc region and, as a result, the ability of Fc receptors to access the Fc-binding site (Fig. 1B).(5,11,12) The deglycosylation of the C_{H2} domain of an IgG1 transforms the horseshoe-like configuration of the native antibody to a closed state, blocking access to the Fc γ R binding site (11,12). As a result, deglycosylated antibodies show reduced binding affinity for Fc γ R. Critically, Fc γ RI is the *only* member of the Fc γ R family that has high affinity for the Fc region and is able to bind monomeric IgGs. The other Fc γ R — Fc γ RII and Fc γ RIII — have lower affinities for monomeric IgGs and prefer to bind to immune-complexes (13). In humans, Fc γ RI is expressed on the surface of monocytes, macrophages, and tissue-resident macrophages, such as Kupffer cells in the liver (5,14). The deglycosylation of antibodies has previously been shown to improve the performance of near-infrared fluorescence imaging agents based on murine antibodies (15).

The core hypothesis of this investigation is that the deglycosylation of antibodies could produce 'immune-silent' radioimmunoconjugates with improved *in vivo* performance. To this end, we produced several DFO-bearing immunoconjugates of the HER2-targeting antibody trastuzumab with differing glycosylation states. Subsequently, we explored the influence of our glycoengineering efforts on the binding of these immunoconjugates with Fc γ RI via SPR, ELISA, and flow cytometry. Finally, we labeled the DFO-bearing immunoconjugates with zirconium-89 (⁸⁹Zr; t_{1/2} ~ 78.4 h; 22.7% β⁺; E_{β+} = 395.5 keV) and explored their *in vivo* behavior in three mouse models of HER2-expressing human breast cancer. A compelling correlation between the *in vitro* and *in vivo* results was observed: the ⁸⁹Zr-DFO-trastuzumab radioimmunoconjugates that

displayed abrogated binding to Fc γ RI *in vitro* exhibited improved performance *in vivo*, specifically decreased uptake in the healthy liver and spleen and increased retention in tumor tissue.

MATERIALS AND METHODS

PET Imaging

PET imaging experiments were conducted on a microPET Focus rodent scanner (Concorde Microsystems). Mice (athymic nude, NSG, or humanized NSG mice) bearing subcutaneous BT474 xenografts (left shoulder, 60-120 mm³, 25-30 days after inoculation) were administered the radioimmunoconjugates [6.5-7.8 MBq (40-60 μ g) in 200 μ L of saline] via tail vein injection (t = 0). Approximately 5 min before PET imaging, mice were anesthetized by inhalation of a 2% isoflurane (Baxter Healthcare):oxygen gas mixture and placed on the scanner bed. Anesthesia was maintained using a 1% isoflurane mixture. PET data for each mouse were recorded via static scans at 24, 48, and 120 h p.i (n = 4 per group). Images were analyzed using ASIPro VM software (Concorde Microsystems). All mouse experiments were performed in accordance with protocols approved by the Institutional Animal Care and Use Committees of Hunter College and MSKCC and followed National Institutes of Health guidelines for animal welfare.

Statistical Analyses

The statistical analyses were performed using GraphPad Prism 7.0 software. All data are expressed as mean \pm SD. When applicable, statistical differences were analyzed by an unpaired, two-tailed Student's t test (with a Welch's correction when mentioned) and the one-way ANOVA for the comparison of more than two groups. Differences at the 95% confidence level (P < 0.05) were considered statistically significant.

RESULTS AND DISCUSSION

Synthesis and Characterization

The HER2-targeting antibody trastuzumab was chosen as a model IgG1 because it is robust, well characterized, and easily available. Furthermore, trastuzumab has been shown to recruit immune effector cells *via* interactions with Fc γ R as part of its therapeutic mechanism (16). ⁸⁹Zr was used as the radionuclide due to its residualizing properties and its physical half-life of ~3.3

days, which is ideally suited to complement the biological half-life of IgG1. Finally, DFO was chosen as the chelator, as it is the “gold standard” chelator for ^{89}Zr in both the laboratory and clinic (17).

The first step in the investigation was the modification of trastuzumab with DFO. To this end, we pursued two different approaches: *non-site-specific* and *site-specific* bioconjugation. The former was achieved via the random — or *non-site-specific* — reaction of an isothiocyanate-bearing variant of DFO (*p*-SCN-Bn-DFO) with the lysines of the antibody (18). The resulting immunoconjugate — DFO-^{nss}trastuzumab — has an average of 1.2 DFO per antibody as estimated by MALDI/ToF. This immunoconjugate was then deglycosylated using two different enzymes (Figs. 2A and 2B). The first, peptide:*N*-glycosidase F (PNGaseF), cleaves the entire glycan chain linked to asparagine at position 297 (Q297), creating a completely deglycosylated immunoconjugate: DFO-^{nss}trastuzumab-PNGaseF. The second, endoglycosidase (EndoS), hydrolyses the chitobiose core of the asparagine-linked glycans, producing a partially deglycosylated immunoconjugate: DFO-^{nss}trastuzumab-EndoS (19).

We also created a *site-specifically* modified, DFO-bearing immunoconjugate via the chemoenzymatic modification of the glycans (Fig. 2B) (20). To this end, trastuzumab was first treated with EndoS and then incubated with the promiscuous galactosyltransferase GalT(Y289L) and the monosaccharide UDP-GalNAz to incorporate azide-bearing sugars into the truncated glycans. Subsequently, DFO was introduced *via* the strain promoted alkyne-azide cycloaddition between DBCO-DFO and the azide-bearing glycans, and a degree-of-labeling (DOL) of 1.3 DFO/mAb was estimated via MALDI-ToF (Supplemental Fig. 1). Critically, in all three cases, the complete removal of glycans was monitored using gel electrophoresis under reducing conditions and confirmed via both a Lens culinaris agglutinin blot *and* MALDI-ToF (Supplemental Figs. 1-3).

***In Vitro* Characterization**

The first step in the *in vitro* evaluation of the immunoconjugates was the assessment of their binding to HER2. SPR revealed that all four immunoconjugates exhibit binding affinities and on- and off-rates with HER2 comparable to that of native trastuzumab (Supplemental Fig. 4 and Supplemental Table 1). Flow cytometry with HER2-positive BT474 cells subsequently

confirmed that the immunoreactivity of all four immunoconjugates is unperturbed (Fig. 3A, Supplemental Fig. 5).

Next, the interactions between the immunoconjugates and Fc γ RI were probed via SPR. Several groups have shown that human IgG₁ exhibit similar interaction patterns with — though different affinities for — human and murine Fc receptors (21,22). Since the *in vivo* behavior of our immunoconjugates would be tested in mice, we decided to investigate their binding to murine Fc γ RI (mFc γ RI) as well as human Fc γ RI (huFc γ RI). Taken together, the SPR data clearly indicate that deglycosylation negatively impacts the interaction between the immunoconjugates and Fc γ RI, though the phenomenon is more pronounced with huFc γ RI than mFc γ RI (Fig. 4, Supplemental Fig. 6, Supplemental Tables 2-5). DFO-^{nss}trastuzumab possesses K_D , on-rate, and off-rate values with huFc γ RI comparable to unmodified trastuzumab (Fig. 4). In contrast, DFO-^{nss}trastuzumab-PNGaseF exhibits a 20-fold reduction in K_D for huFc γ RI compared to native trastuzumab as well as a dramatically accelerated off-rate. Interestingly, the two EndoS-modified immunoconjugates — DFO-^{nss}trastuzumab-EndoS and DFO-^{ss}trastuzumab-EndoS — present intermediate cases, with K_D values and off-rates between that of native trastuzumab and DFO-^{nss}trastuzumab-PNGaseF. The impact of deglycosylation on the huFc γ RI binding of the immunoconjugates is reinforced by the dramatic decreases in the half-life of the interaction between the two components: DFO-^{nss}trastuzumab boasts a half-life of 86.1 ± 9.6 min with huFc γ RI, a value which decreases to 15.4 ± 0.5 for DFO-^{ss}trastuzumab-EndoS and 5.4 ± 0.2 for DFO-^{nss}trastuzumab-PNGaseF.

Moving on to mFc γ RI, native trastuzumab displays a ~10-fold lower binding affinity (~37 nM) for mFc γ RI compared to huFc γ RI (~3 nM), a result that is in agreement with the wider literature (Supplemental Fig. 6 and Supplemental Tables 4 and 5) (13,21-24). Yet still, the EndoS-treated immunoconjugates exhibit decreased K_D values and accelerated off-rates compared to native trastuzumab. Surprisingly, DFO-^{nss}trastuzumab-PNGaseF displays a K_D similar to that of unmodified trastuzumab. Yet it is important to note that this value is not representative of the true behavior of the immunoconjugate with mFc γ RI. Since $K_D = k_d/k_a$, this seemingly strong binding affinity is most likely the product of a high off-rate and an equally fast on-rate. In light of this, the half-lives of the immunoconjugates with mFc γ RI likely provides the most complete picture of their interaction with the receptor. The half-lives of all five constructs with mFc γ RI are significantly shorter than the analogous values for their interaction with

huFcγRI. However, the values for the three deglycosylated immunoconjugates are significantly shorter than those of DFO-^{nss}trastuzumab and native trastuzumab, with DFO-^{nss}trastuzumab-PNGaseF having the shortest half-life of all.

These relationships between deglycosylation and FcγRI binding are reinforced by ELISA and *in vitro* binding assays. ELISA data with huFcγRI clearly indicate that DFO-^{nss}trastuzumab-PNGaseF, DFO-^{nss}trastuzumab-EndoS, and DFO-^{ss}trastuzumab-EndoS all exhibit decreased binding to huFcγRI compared to DFO-^{nss}trastuzumab and native trastuzumab (Fig. 3B and Supplemental Fig. 7). Significantly higher concentrations of the immunoconjugates (50 μg/mL) had to be used to evaluate mFcγRI binding via ELISA, though similar patterns were uncovered: the deglycosylated constructs all have attenuated binding to mFcγRI compared to the parent constructs (Fig. 3B). Next, because both huFcγRI and mFcγRI can be found on the surface of macrophages, a murine macrophage cell line (RAW 264.7) as well as a human lymphoma cell line differentiated into mature macrophages (U937) were selected for flow cytometry experiments (Figs. 3C and Supplemental Figs. 8 and 9) (14,25). As one might expect based on the ELISA and SPR data, DFO-^{nss}trastuzumab-PNGaseF, DFO-^{nss}trastuzumab-EndoS, and DFO-^{ss}trastuzumab-EndoS all displayed decreased binding to both murine and human macrophages.

In Vivo Behavior

The next step in the investigation was interrogating the *in vivo* behavior of the deglycosylated immunoconjugates. Given the exigencies of *in vivo* preclinical work, two of the immunoconjugates bearing modified glycans — DFO-^{nss}trastuzumab-PNGaseF and DFO-^{ss}trastuzumab-EndoS — were chosen for *in vivo* evaluation alongside their more traditional analog, DFO-^{nss}trastuzumab. Our logic here was simple: the former possesses the shortest half-lives with both huFcγRI and mFcγRI, and the latter offers the dual advantages of site-specific bioconjugation *and* attenuated binding to huFcγRI and mFcγRI. These immunoconjugates were radiolabeled with ⁸⁹Zr via standard protocols, producing a trio of radioimmunoconjugates in >95% radiochemical yield and >99% radiochemical purity with specific activities of 81.4 – 99.9 MBq/mg. The stability of the radioimmunoconjugates was tested in human serum at 37 °C, and all three demonstrated >85% stability after 7 days (Supplemental Fig. 10).

We conducted the initial *in vivo* evaluation of these radioimmunoconjugates in athymic nude mice because they are the most commonly used immunodeficient strain used for xenograft models of human cancer. Furthermore, nude mice possess immune effector cells that express the murine Fc γ RI receptor, including macrophages, natural killer cells, and dendritic cells (26). The *in vivo* performance of the radioimmunoconjugates was evaluated via PET imaging experiments as well as biodistribution studies in mice bearing subcutaneous HER2-expressing BT474 human breast cancer xenografts. PET images were collected at 24, 48, and 120 h after the injection of the radioimmunoconjugates (7.0-7.8 MBq, 70-80 μ g). At the earliest time point (24 h), the images revealed that all 3 radioimmunoconjugates accumulated in the HER2-positive tumors. In addition, ^{89}Zr -DFO-^{nss}trastuzumab, ^{89}Zr -DFO-^{ss}trastuzumab-EndoS, and ^{89}Zr -DFO-^{nss}trastuzumab-PNGaseF all produced background signal in the heart and liver, the latter creating the lowest activity concentrations in these tissues (Fig. 5A). Over the course of the experiment, the background uptake decreased for all three radioimmunoconjugates in favor of higher tumoral activity concentrations. The biodistribution data tell a similar story (Supplemental Fig. 11 and Supplemental Table 6). Taken together, these data clearly suggest that deglycosylation with PNGaseF and site-specific modification using EndoS had produced radioimmunoconjugates with *in vivo* behavior comparable to that of traditional ^{89}Zr -DFO-^{nss}trastuzumab.

Our findings in athymic nude mice did little to support our initial hypothesis. However, Overdijk *et al.* have previously cautioned that the activation of cellular immune effector functions by hIgG1 might be underestimated in mice due to differences between mFc γ RI and huFc γ RI (21,22). Armed with this knowledge, we sought a more advantageous model to highlight the impact of deglycosylation on the biodistribution of our radioimmunoconjugates. To this end, we turned to a highly immunodeficient strain: NOD *scid* gamma (NOD.Cg-*Prkdc^{scid}Il2rg^{tm1Wjl}/SzJ*), or NSG, mice. This strain of mice lacks endogenous immunoglobulins that can compete with radioimmunoconjugates for unoccupied mFc γ RI on myeloid cells such as monocytes, neutrophils, and eosinophils, as well as tissue-resident macrophages in the liver, spleen, and bone (27).

For these experiments, NSG mice bearing subcutaneous HER2-expressing BT474 xenografts were injected *via* tail vein with the three radioimmunoconjugates (6.5-7.4 MBq, 60-80 μ g) and imaged after 24, 48, and 120 h (Fig. 5B). PET imaging with all three radioimmunoconjugates clearly delineated the BT474 xenografts as early as 24 h post-injection. However, besides high

activity concentrations in the heart and blood vessels, a marked difference was apparent in the images produced by the 3 radioimmunoconjugates: $^{89}\text{Zr-DFO-}^{\text{nss}}$ trastuzumab produced very high activity concentrations in the liver, while the pair of glycans-modified radioimmunoconjugates yielded far lower uptake in the organ. By 120 h p.i., the tumor was the most prominent feature in the scans collected with $^{89}\text{Zr-DFO-}^{\text{nss}}$ trastuzumab-PNGaseF and $^{89}\text{Zr-DFO-}^{\text{ss}}$ trastuzumab-EndoS, while the images produced by $^{89}\text{Zr-DFO-}^{\text{nss}}$ trastuzumab-DFO show dramatically lower tumoral uptake as well as significant off-target activity concentrations in the liver and bone. Interestingly, over the course of the experiment, the clearance of $^{89}\text{Zr-DFO-}^{\text{nss}}$ trastuzumab-PNGaseF from the heart and blood vessels appeared slower than either of the two other radioimmunoconjugates, an observation consistent with the idea of an “immune-silent” radioimmunoconjugate.

The differences between the *in vivo* performance of $^{89}\text{Zr-DFO-}^{\text{nss}}$ trastuzumab-PNGaseF and $^{89}\text{Zr-DFO-}^{\text{nss}}$ trastuzumab were confirmed by biodistribution studies (Fig. 6). At 120 h p.i., the tumoral activity concentration produced by $^{89}\text{Zr-DFO-}^{\text{nss}}$ trastuzumab-PNGaseF (87.7 ± 5.9 %ID/g) was significantly higher than that created by $^{89}\text{Zr-DFO-}^{\text{nss}}$ trastuzumab (7.9 ± 3.3 %ID/g; Fig. 6 and Supplemental Table 7). Simultaneously, the activity concentrations in the liver and spleen of the NSG mice injected with the fully deglycosylated immunoconjugate were reduced by 3- and 9-fold respectively. These two trends yield dramatically improved tumor-to-liver and tumor-to-spleen activity concentration ratios for $^{89}\text{Zr-DFO-}^{\text{nss}}$ trastuzumab-PNGaseF (17.0 ± 2.5 and 12.3 ± 0.9 , respectively) compared to $^{89}\text{Zr-DFO-}^{\text{nss}}$ trastuzumab (0.5 ± 0.2 and 0.1 ± 0.1 , respectively) (Supplemental Table 7). However, the persistence of the deglycosylated radioimmunoconjugate in the blood yielded lower tumor-to-blood activity concentration ratios for $^{89}\text{Zr-DFO-}^{\text{nss}}$ trastuzumab-PNGaseF compared to $^{89}\text{Zr-DFO-}^{\text{nss}}$ trastuzumab: 11.4 ± 2.8 vs 112.7 ± 67.7 at 120 h p.i. (Supplemental Table 8). Likewise, highly perfused organs such as the heart and lungs also exhibited decreased tumor-to-background activity concentration ratios with $^{89}\text{Zr-DFO-}^{\text{nss}}$ trastuzumab-PNGaseF, almost certainly due to the persistence of the radioimmunoconjugate in the blood. $^{89}\text{Zr-DFO-}^{\text{ss}}$ trastuzumab-EndoS proved to be an intermediate case. Briefly, the site-specifically modified immunoconjugate showed higher tumoral uptake values (*e.g.* 53.9 ± 11.0 at 120 h post-injection) than $^{89}\text{Zr-DFO-}^{\text{nss}}$ trastuzumab but higher activity concentrations in the liver and spleen than $^{89}\text{Zr-DFO-}^{\text{nss}}$ trastuzumab-PNGaseF.

Ultimately, while NSG mice allow us to demonstrate the benefit of using deglycosylated “immune-silent” antibodies for immunoPET, the NSG platform is an exaggerated

immunodeficient model with little clinical relevance. To wit, while nude mice have serum total IgG titers $>40 \mu\text{g/mL}$, the IgG titers in NSG mice are almost undetectable (27). In contrast, human patients possess endogenous immunoglobulins that occupy huFc γ RI on immune effector cells. This, of course, has the potential to abrogate the benefits provided by immune-silent radioimmunoconjugates that we have seen in the NSG mice.

Having evaluated our immunoconjugates in two different immunodeficient strains of mice, we were eager to test our hypothesis in a more clinically relevant model. To this end, we next characterized the *in vivo* behavior of our radioimmunoconjugates in humanized mice. Specifically, we used NSG mice that were sub-lethally irradiated at 3 weeks after birth and subsequently reconstituted with human hematopoietic stem cells derived from cord blood in order to express a functional human immune system, including human B cells, T cells, NK cells, dendritic cells, and monocytes (28,29). The last entry in this list is particularly important, as monocytes are the primary human immune system cells expressing Fc γ RI(14). Importantly, a titration of the serum from these mice confirmed the presence of endogenous human IgG ($202 \pm 67 \mu\text{g/mL}$) in levels consistent with published data on the strain (Supplemental Fig. 12) (28,30).

Given the high cost of humanized mice, we chose to compare a pair of radioimmunoconjugates: the control $^{89}\text{Zr-DFO-}^{\text{nss}}$ trastuzumab and the deglycosylated $^{89}\text{Zr-DFO-}^{\text{nss}}$ trastuzumab-PNGaseF. To this end, humanized NSG mice (huNSG) bearing subcutaneous HER2-positive BT474 human breast cancer xenografts were injected with the radioimmunoconjugates (6.8-7.4 MBq), and PET imaging was performed after 24, 48, and 120 h. Images obtained with both radioimmunoconjugates display a clear delineation of tumors as early as 24 h p.i., though the tumoral activity concentrations produced by $^{89}\text{Zr-DFO-}^{\text{nss}}$ trastuzumab-PNGaseF are far higher than those produced by $^{89}\text{Zr-DFO-}^{\text{nss}}$ trastuzumab (Fig. 7A). However, the patterns of non-specific uptake created by the two immunoconjugates were dramatically different. $^{89}\text{Zr-DFO-}^{\text{nss}}$ trastuzumab-PNGaseF exhibited relatively high activity concentrations in the heart throughout the experiment but very low accumulation in any other non-target tissues. $^{89}\text{Zr-DFO-}^{\text{nss}}$ trastuzumab, in contrast, produced lower activity concentrations in the heart and blood vessels but far higher levels of uptake in the liver, spleen, and bones. These differences are particularly striking in the maximum intensity projections collected at 120 h post-injection. For $^{89}\text{Zr-DFO-}^{\text{nss}}$ trastuzumab-PNGaseF, the only visible feature is the tumor. For $^{89}\text{Zr-DFO-}^{\text{nss}}$

^{nss}trastuzumab, the tumor boasts the highest uptake, but the liver, spleen, and bones are prominent as well.

The differences between the *in vivo* performances of the two radioimmunoconjugates were further illustrated by a biodistribution study performed at 120 h p.i. (Fig. 7B, Supplemental Fig. 13, Supplemental Table 9). The deglycosylated radioimmunoconjugate (⁸⁹Zr-DFO-^{nss}trastuzumab-PNGaseF) produced nearly double the tumoral activity concentration created by ⁸⁹Zr-DFO-^{nss}trastuzumab: 102.1 ± 18.5 %ID/g vs. 48.4 ± 22.5 %ID/g. Furthermore, ⁸⁹Zr-DFO-^{nss}trastuzumab-PNGaseF yielded much lower uptake in the liver, spleen and bone. ⁸⁹Zr-DFO-^{nss}trastuzumab-PNGaseF produced much higher activity concentrations in the blood as well as highly perfused organs such as the lungs and heart. This observation can be attributed to the persistence of the radioimmunoconjugate in systemic circulation, behavior in line with the notion of an ‘immune-silent’ radioimmunoconjugate. Taken together, these *in vivo* data underscore the improved performance of the deglycosylated radioimmunoconjugate relative to its more traditional, fully glycosylated analog. Indeed, ⁸⁹Zr-DFO-^{nss}trastuzumab-PNGaseF produced high tumor-to-background activity concentration ratios and excellent immunoPET images despite the presence of a fully reconstituted human immune system and the endogeneous IgGs in huNSG mice. While ⁸⁹Zr-DFO-^{nss}trastuzumab enabled the visualization of tumor tissue, it was also subject to Fc/FcγR-mediated uptake in non-target organs such as the liver, spleen, and bones.

Before we delve into the implications of this work, it is important to issue four caveats. First, further investigations into the generality of this phenomenon are certainly warranted. Second, although humanized mice were used as a surrogate to study the impact of the *in vivo* interaction between humanized IgG1 and the human immune system, it is important to note that this model has its limitations (31). Specifically, the titers of endogenous human IgGs in this mouse model are significantly lower than in immunocompetent mouse strains due to the lack of class switching from IgM to IgG isotypes *in vivo*. This might be attributed to the lack of B-cell maturation in the humanized mouse model due to the absence of functional lymph nodes, germinal centers, and follicular dendritic cells (32,33). Third, physiology-based pharmacokinetic models suggest that Fc/FcγR interactions do not impact the *in vivo* biodistribution of antibody-based imaging agents and drugs due to the occupancy of FcγR sites by the preexisting pool of endogenous immunoglobulins (34). And finally, it is also important to note that non-specific uptake of radioimmunoconjugates in the liver is not solely mediated by FcγRI. To wit, aggregated

antibodies are also routed to the liver, and in presence of shed antigens, the formation of soluble immunocomplexes can be another cause of this off-target signal. In these cases, deglycosylation may not be of any help for improving imaging quality.

Ultimately, we believe that this work could have an impact in both the laboratory and the clinic. These data clearly suggest that deglycosylation is an inexpensive, effective, and modular approach to improving the quality of immunoPET images collected in preclinical models of cancer. Indeed, we believe that this strategy could be particularly useful in studies using highly immunodeficient mice or humanized mouse models. Furthermore, the benefits of deglycosylation can be coupled with the advantages of site-specific labeling by employing the EndoS-based bioconjugation strategy that we have described here.

The clinical implications of this work are admittedly less clear. Patients undergoing immunoPET scans are routinely pre- or co-dosed with an excess of unlabeled target-specific antibody (*e.g.* ~48 mg of trastuzumab alongside ~2 mg of ⁸⁹Zr-DFO-trastuzumab) (35). This practice consistently improves the contrast of images by decreasing the uptake of the radioimmunoconjugate in healthy non-target organs, specifically the liver. If the root of this phenomenon lies in the ability of the unlabeled antibody to saturate FcγRI binding sites in non-target organs, the use of deglycosylated radioimmunoconjugates could offer a cheaper and easier means to the same ends, thereby enabling the more sensitive detection of metastases in the liver and other non-target organs. On the other hand, as we've noted above, higher endogenous IgG levels may preclude the benefits of deglycosylation in most patients. In this case, deglycosylated radioimmunoconjugates could still prove valuable for immunoPET in patients — including recent recipients of chemotherapy or radiation therapy — with low B-cell counts (36).

CONCLUSION

In this work, we have interrogated the role of Fc/FcγRI interactions on the *in vivo* performance of antibody-based PET imaging agents. Our findings suggest that the binding of humanized IgG1 by FcγRI contributes to the uptake of radioimmunoconjugates in non-target tissues during immunoPET imaging. As a result, we hypothesized that attenuating these Fc/FcγRI interactions *via* the use of deglycosylated radioimmunoconjugates could be a viable strategy for decreasing unwanted uptake in healthy organs. We have demonstrated that deglycosylated radioimmunoconjugates not only exhibit decreased affinity for FcγRI but also

produce both lower activity concentrations in non-target organs and higher activity concentrations in tumor tissue in NSG and huNSG mice compared to a fully glycosylated analogue. In the end, these findings suggest that deglycosylation is a facile, inexpensive, and versatile approach to the creation of “immune-silent” radioimmunoconjugates that could be more effective imaging agents than traditional radiolabeled antibodies in a wide variety of preclinical studies as well as certain clinical patient populations. We look forward to further exploring the implications of this finding for immunoPET as well as interrogating the ramifications that these findings may have in the context of antibody-drug conjugates and therapeutic radioimmunoconjugates.

ACKNOWLEDGEMENTS

The authors are grateful for the generous financial support of the National Institutes of Health (BMZ; R01CA204167) and the Tow Foundation (SKS). Services provided by the MSKCC Small-Animal Imaging Core Facility were supported in part by NIH grants R24 CA83084 and P30 CA08748.

REFERENCES

1. Wu AM. Antibodies and antimatter: The resurgence of immuno-PET. *J Nucl Med.* 2009;50:2-5.
2. Pyzik M, Rath T, Lencer WI, Baker K, Blumberg RS. FcRn: The architect behind the immune and nonimmune functions of IgG and albumin. *J Immunol.* 2015;194:4595-4603.
3. Nimmerjahn F, Ravetch JV. Fcγ receptors as regulators of immune responses. *Nat Rev Immunol.* 2008;8:34-47.
4. Sockolosky JT, Szoka FC. The neonatal Fc receptor, FcRn, as a target for drug delivery and therapy. *Adv Drug Del Rev.* 2015;91:109-124.
5. Pincetic A, Bournazos S, DiLillo DJ, et al. Type I and type II Fc receptors regulate innate and adaptive immunity. *Nat Immunol.* 2014;15:707-716.
6. Leelawattanachai J, Kwon KW, Michael P, Ting R, Kim JY, Jin MM. Side-by-side comparison of commonly used biomolecules that differ in size and affinity on tumor uptake and internalization. *PLoS One.* 2015;10:e0124440.
7. Hezareh M, Hessell AJ, Jensen RC, van de Winkel JGJ, Parren PWI. Effector function activities of a panel of mutants of a broadly neutralizing antibody against human immunodeficiency virus type 1. *J Virol.* 2001;75:12161-12168.
8. Sondermann P, Szymkowski DE. Harnessing Fc receptor biology in the design of therapeutic antibodies. *Curr Opin Immunol.* 2016;40:78-87.
9. Raju TS, Briggs JB, Borge SM, Jones AJ. Species-specific variation in glycosylation of IgG: evidence for the species-specific sialylation and branch-specific galactosylation and importance for engineering recombinant glycoprotein therapeutics. *Glycobiology.* 2000;10:477-486.
10. Liu L. Antibody glycosylation and its impact on the pharmacokinetics and pharmacodynamics of monoclonal antibodies and Fc-fusion proteins. *J Pharm Sci.* 2015;104:1866-1884.
11. Baruah K, Bowden TA, Krishna BA, Dwek RA, Crispin M, Scanlan CN. Selective deactivation of serum IgG: A general strategy for the enhancement of monoclonal antibody receptor interactions. *J Mol Biol.* 2012;420:1-7.
12. Borrok MJ, Jung ST, Kang TH, Monzingo AF, Georgiou G. Revisiting the role of glycosylation in the structure of human IgG Fc. *ACS Chem Biol.* 2012;7:1596-1602.
13. Bruhns P, Iannascoli B, England P, et al. Specificity and affinity of human Fcγ receptors and their polymorphic variants for human IgG subclasses. *Blood.* 2009;113:3716-3725.
14. Tuijnman WB, Van Wichen DF, Schuurman H-J. Tissue distribution of human IgG Fc receptors CD16, CD32 and CD64: An immunohistochemical study. *APMIS.* 1993;101:319-329.
15. Gao P, Pinkston KL, Wilganowski N, et al. Deglycosylation of mAb by EndoS for improved molecular imaging. *Mol Imaging Biol.* 2015;17:195-203.
16. Shi Y, Fan X, Deng H, et al. Trastuzumab triggers phagocytic killing of high HER2 cancer cells in vitro and in vivo by interaction with Fcγ receptors on macrophages. *J Immunol.* 2015;194:4379-4386.
17. Deri MA, Zeglis BM, Francesconi LC, Lewis JS. PET imaging with ⁸⁹Zr: From radiochemistry to the clinic. *Nucl Med Biol.* 2013;40:3-14.

18. Perk LR, Vosjan MJ, Visser GW, et al. p-Isothiocyanatobenzyl-desferrioxamine: a new bifunctional chelate for facile radiolabeling of monoclonal antibodies with zirconium-89 for immuno-PET imaging. *Eur J Nucl Med Mol Imaging*. 2010;37:250-259.
19. Collin M, Olsén A. EndoS, a novel secreted protein from *Streptococcus pyogenes* with endoglycosidase activity on human IgG. *EMBO J*. 2001;20:3046-3055.
20. Zeglis BM, Davis CB, Aggeler R, et al. Enzyme-mediated methodology for the site-specific radiolabeling of antibodies based on catalyst-free click chemistry. *Bioconjugate Chem*. 2013;24:1057-1067.
21. Dekkers G, Bentlage AEH, Stegmann TC, et al. Affinity of human IgG subclasses to mouse Fc gamma receptors. *mAbs*. 2017;9:767-773.
22. Overdijk MB, Verploegen S, Ortiz Buijsse A, et al. Crosstalk between human IgG isotypes and murine effector cells. *J Immunol*. 2012;189:3430-3438.
23. Bruhns P. Properties of mouse and human IgG receptors and their contribution to disease models. *Blood*. 2012;119:5640-5649.
24. Canfield SM, Morrison SL. The binding affinity of human IgG for its high affinity Fc receptor is determined by multiple amino acids in the CH2 domain and is modulated by the hinge region. *J Exp Med*. 1991;173:1483-1491.
25. Jayaram Y, Buckle AM, Hogg N. The Fc receptor, FcRI, and other activation molecules on human mononuclear phagocytes after treatment with interferon-gamma. *Clin Exp Immunol*. 1989;75:414-420.
26. Guillemins M, Bruhns P, Saeys Y, Hammad H, Lambrecht BN. The function of Fc γ receptors in dendritic cells and macrophages. *Nat Rev Immunol*. 2014;14:349.
27. Sharma SK, Chow A, Monette S, et al. Fc-mediated anomalous biodistribution of therapeutic antibodies in immunodeficient mouse models. *Cancer Res*. 2018;78:1820-1832.
28. Ishikawa F, Yasukawa M, Lyons B, et al. Development of functional human blood and immune systems in NOD/SCID/IL2 receptor γ chain(null) mice. *Blood*. 2005;106:1565-1573.
29. Baerenwaldt A, Lux A, Danzer H, et al. Fc γ receptor IIB (Fc γ RIIB) maintains humoral tolerance in the human immune system in vivo. *Proc Natl Acad Sci U S A*. 2011;108:18772-18777.
30. Ito M, Shiina M, Saito Y, Tokuda Y, Kametani Y, Habu S. Antigen-specific antibody production of human B cells in NOG mice reconstituted with the human immune system. In: Nomura T, Watanabe T, Habu S, eds. *Humanized Mice*. Berlin, Heidelberg: Springer Berlin Heidelberg; 2008:95-107.
31. Shultz LD, Ishikawa F, Greiner DL. Humanized mice in translational biomedical research. *Nat Rev Immunol*. 2007;7:118-130.
32. Brehm MA, Shultz LD, Luban J, Greiner DL. Overcoming current limitations in humanized mouse research. *J Infect Dis*. 2013;208 Suppl 2:S125-130.
33. Chen Q, He F, Kwang J, Chan JK, Chen J. GM-CSF and IL-4 stimulate antibody responses in humanized mice by promoting T, B, and dendritic cell maturation. *J Immunol*. 2012;189:5223-5229.
34. Abuqayyas L, Balthasar JP. Application of knockout mouse models to investigate the influence of Fc gamma R on the tissue distribution and elimination of 8C2, a murine IgG1 monoclonal antibody. *Int J Pharm*. 2012;439:8-16.

35. Dijkers EC, Oude Munnink TH, Kosterink JG, et al. Biodistribution of ^{89}Zr -trastuzumab and PET imaging of HER2-positive lesions in patients with metastatic breast cancer. *Clin Pharmacol Ther.* 2010;87:586-592.
36. Verma R, Foster RE, Horgan K, et al. Lymphocyte depletion and repopulation after chemotherapy for primary breast cancer. *Breast Cancer Res.* 2016;18:10.

FIGURES AND FIGURE CAPTIONS

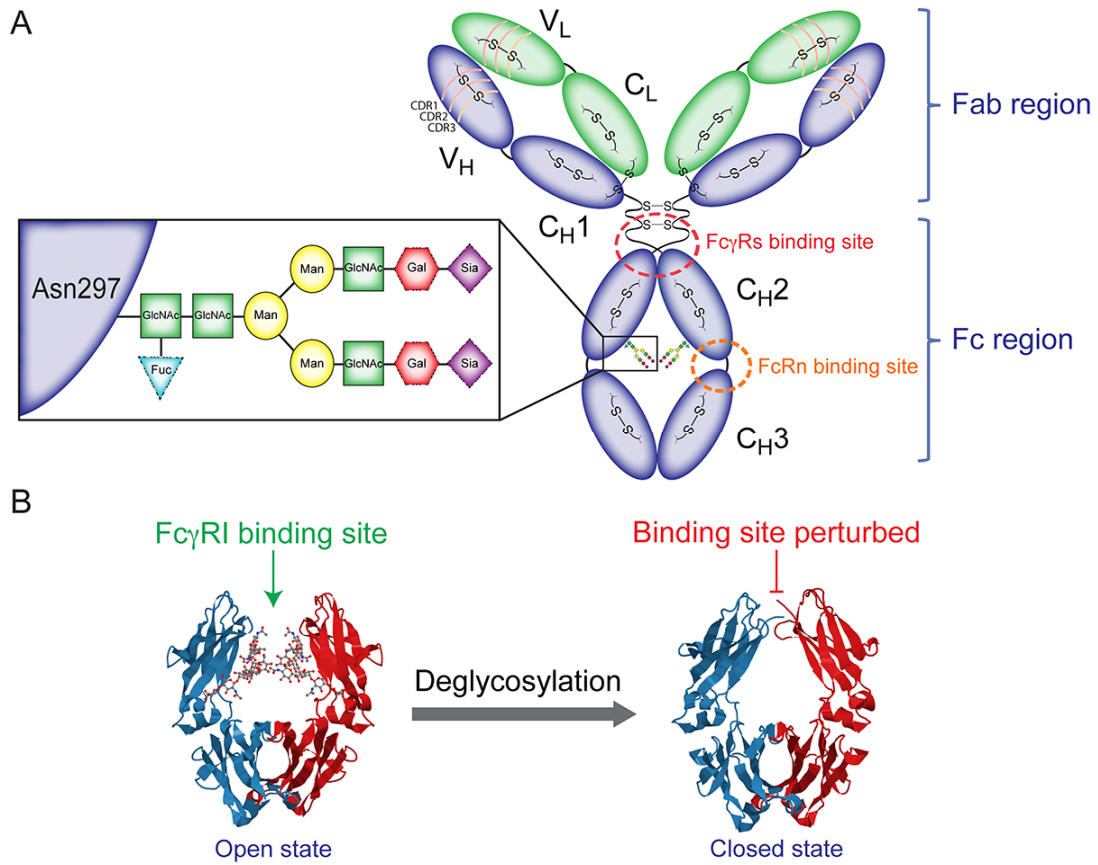


Figure 1. Antibody structure and FcγRI binding. (A) Detailed structure of an antibody with a magnified view of the glycans. (B) Cartoon depicting the influence of deglycosylation on the structure of the Fc region of an antibody and its binding to FcγRI.

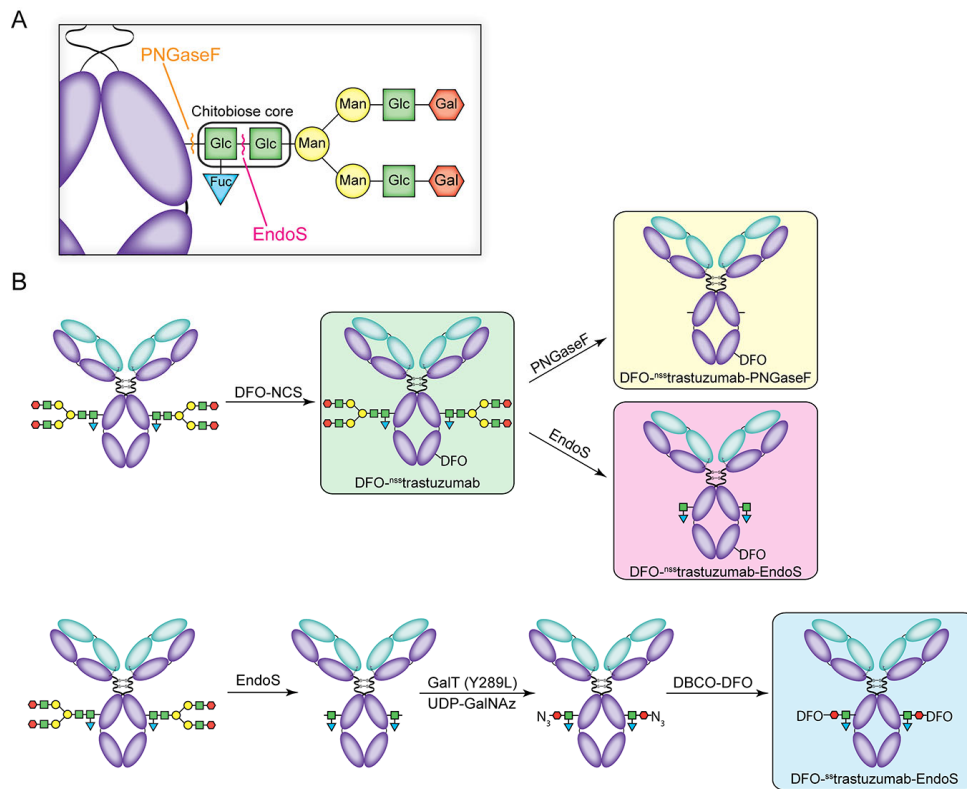


Figure 2. The preparation of the trastuzumab immunoconjugates. (A) Magnified view of the cleavage sites for PNGaseF and EndoS. (B) Scheme of the synthesis of the non-site-specifically and site-specifically modified immunoconjugates.

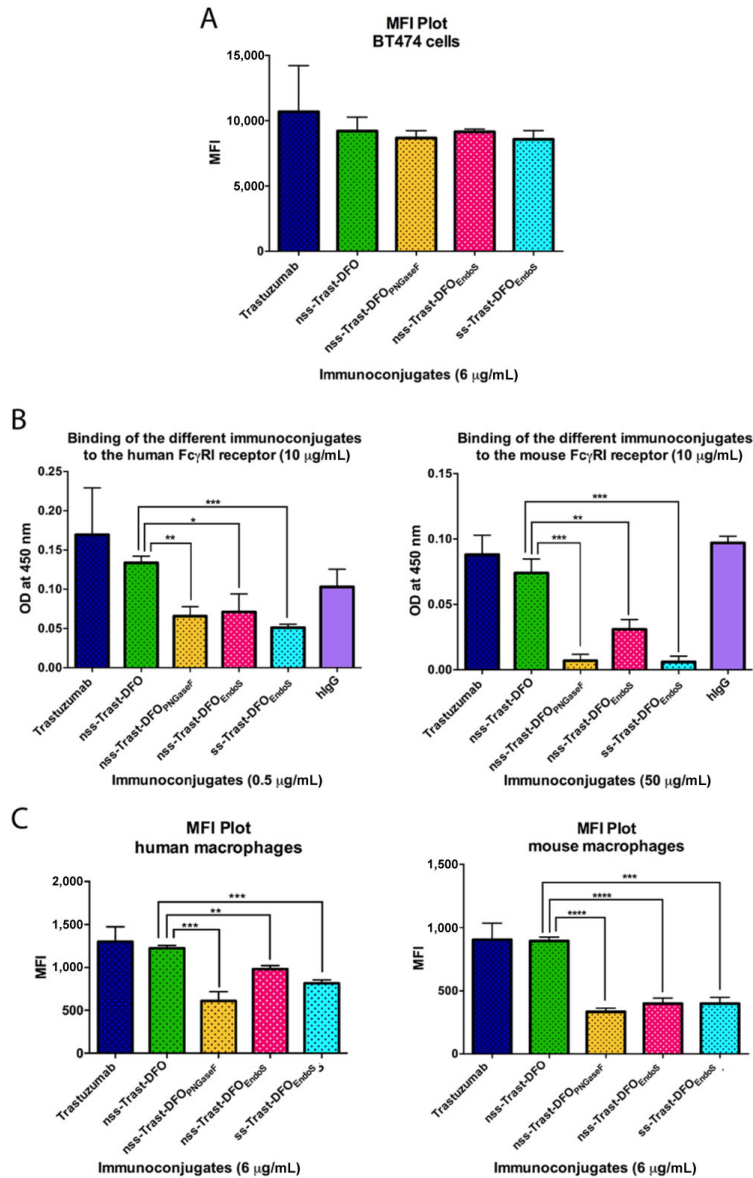


Figure 3. Flow cytometry and ELISA analyses of the DFO-bearing immunoconjugates. (A) Flow cytometry with BT474 cells to verify HER2-binding. (B) ELISA of the immunoconjugates (0.5 or 50 µg/ml) with huFc γ RI (10 µg/ml) and mFc γ RI (10 µg/ml). (C) Flow cytometry of the immunoconjugates with human U937 macrophages and mouse RAW 264.7 macrophages. Data represents mean \pm SD; each immunoconjugate was tested in triplicate (distinct samples). (MFI = Mean Fluorescence Intensity). Data were analyzed by the unpaired, two-tailed Student's t test: * $p < 0.05$, ** $p < 0.01$, *** $p < 0.001$, **** $p < 0.0001$.

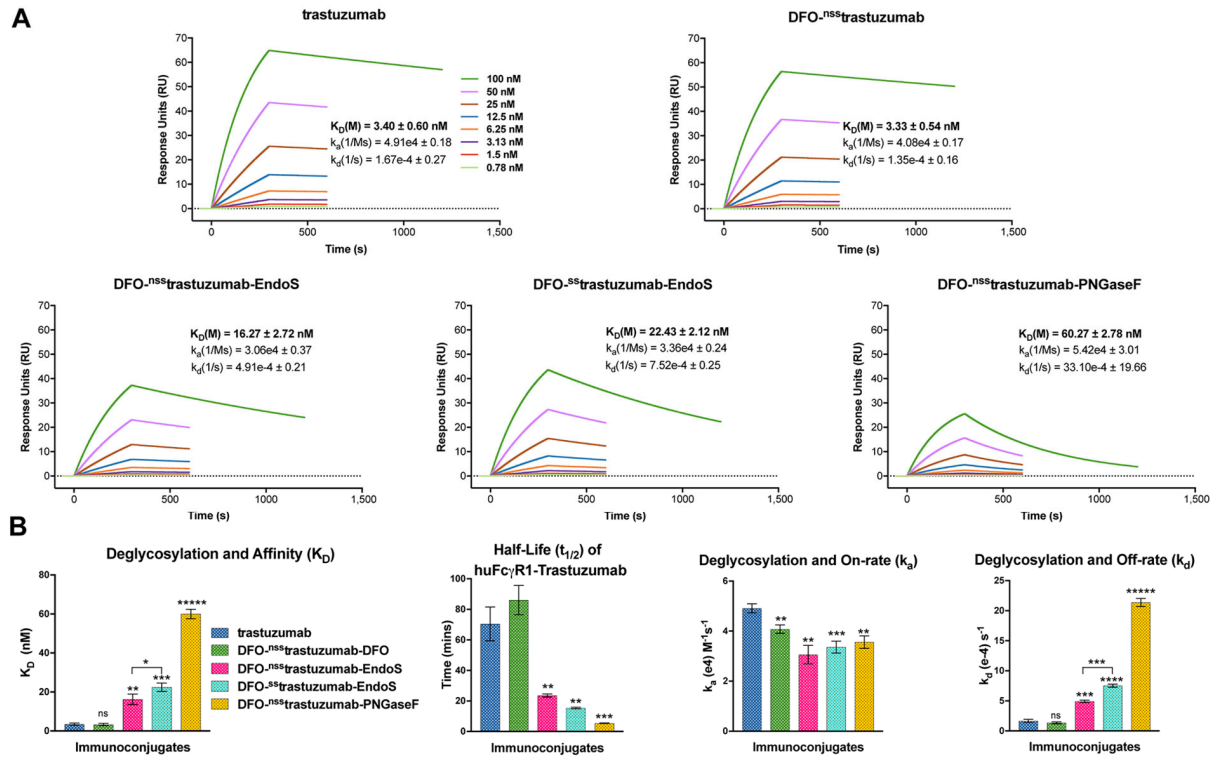


Figure 4. SPR analysis of the interaction between the immunoconjugates and recombinant huFc γ RI. (A) The binding affinity and kinetic rate constants for each immunoconjugate are shown in the sensorgram plots. (B) Bar graphs illustrating the correlation between deglycosylation and binding affinity (K_D), half-life ($t_{1/2}$), on-rate (k_a) and off-rate (k_d). Statistically significant relationships are indicated with asterisks. * = $p < 0.05$, ** = $p < 0.005$, *** = $p < 0.0005$, **** = $p < 0.00005$, ***** = $p < 0.000005$.

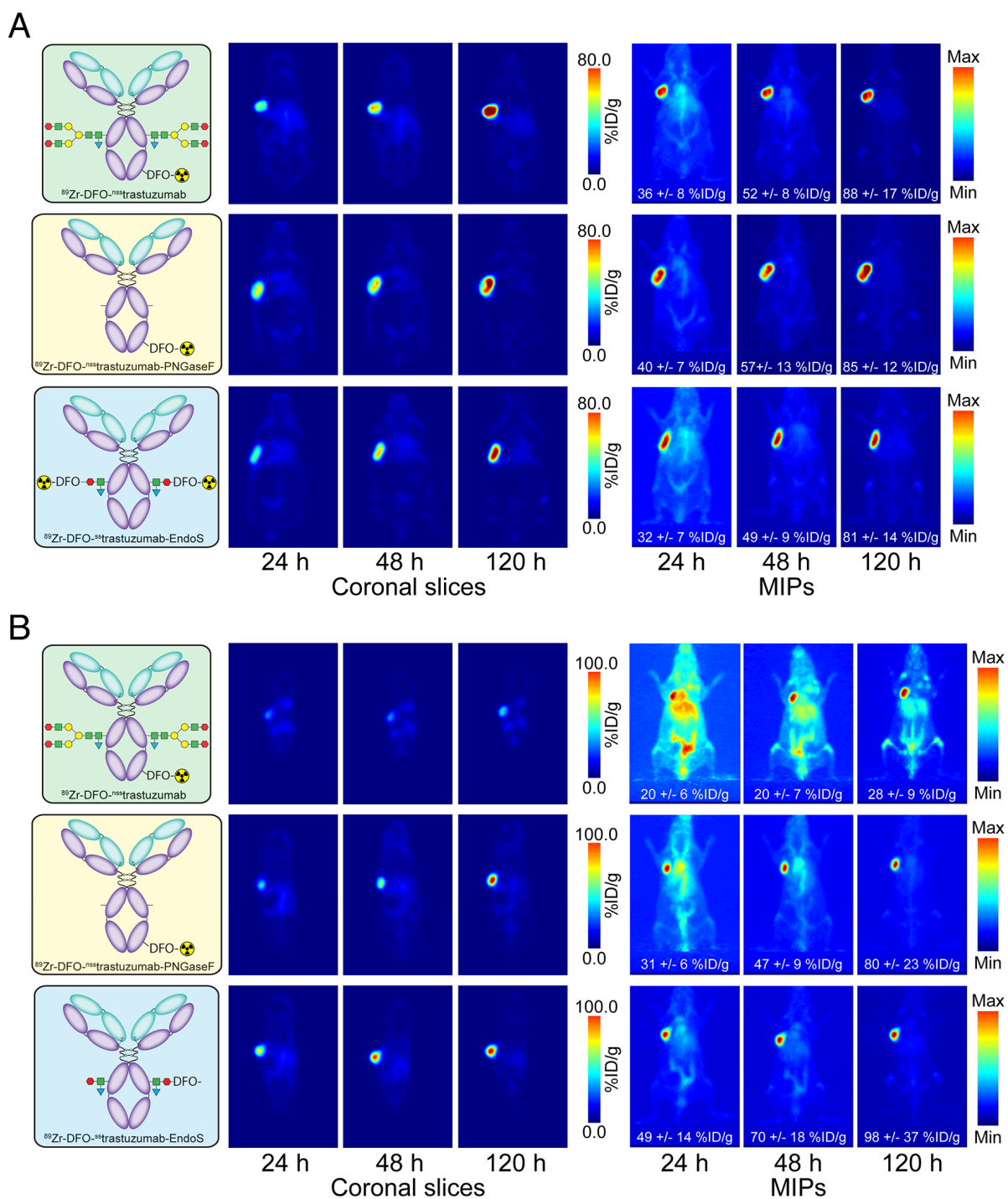


Figure 5. PET imaging in nude and NSG mice. Planar (left) and maximum intensity projection (MIP, right) PET images of (A) nude and (B) NSG mice bearing subcutaneous BT474 xenografts at 24, 48, and 120 h post-injection. The values in white represent tumoral activity concentrations in %ID/g \pm S.D. as determined via region-of-interest analysis (n = 4).

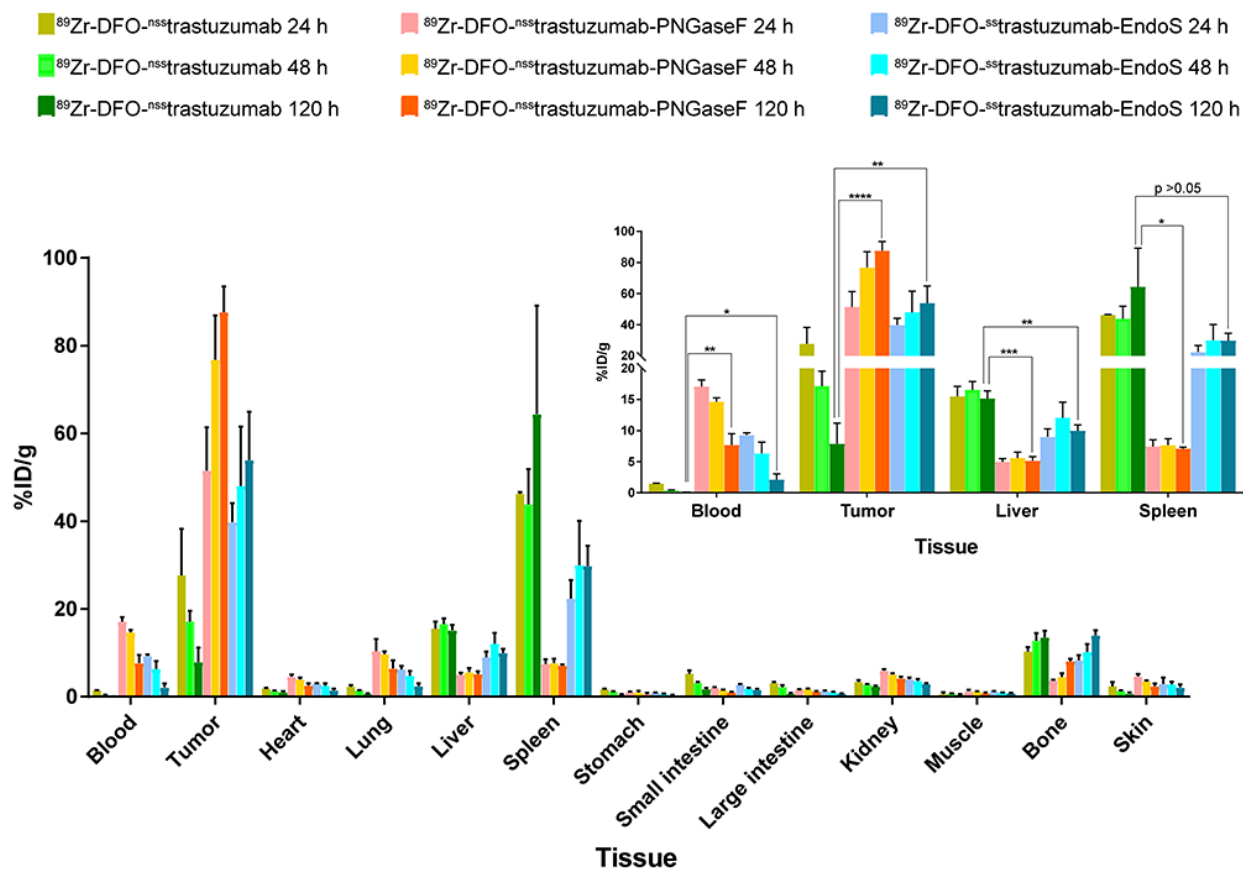


Figure 6. *In vivo* biodistribution profile for ^{89}Zr -DFO- $^{nss+}$ trastuzumab, ^{89}Zr -DFO- $^{nss+}$ trastuzumab-PNGaseF, and ^{89}Zr -DFO- $^{ss+}$ trastuzumab-EndoS at 24, 48, and 120 h post-injection in NSG mice bearing subcutaneous BT474 xenografts. Data represents mean \pm SD, $n = 4$. Data were analyzed by the one-way ANOVA: * $p < 0.05$, ** $p < 0.01$, *** $p < 0.001$, **** $p < 0.0001$.

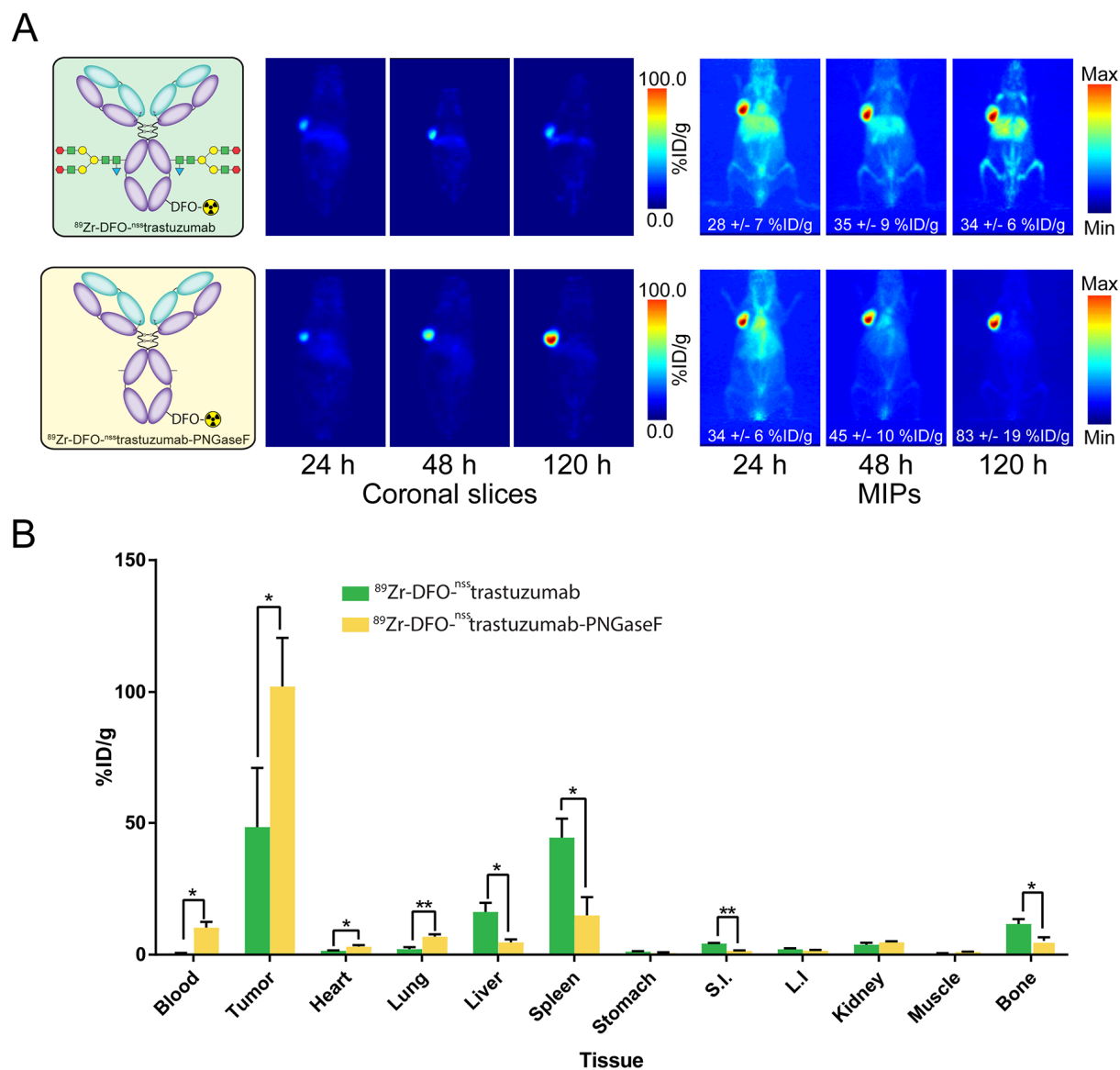


Figure 7. *In vivo* results in humanized NSG mice. (A) Planar (left) and maximum intensity projection (MIP, right) PET images of humanized NSG mice bearing subcutaneous BT474 xenografts at 24, 48, and 120 h post-injection. The values in white represent tumoral activity concentrations in %ID/g \pm S.D. as determined via region-of-interest analysis (n = 4). (B) *In vivo* biodistribution profile for $^{89}\text{Zr-DFO-nss-trastuzumab}$ and $^{89}\text{Zr-DFO-nss-trastuzumab-PNGaseF}$ at 120 h post-injection in humanized NSG mice bearing BT474 tumors. Data represents mean \pm SD, n = 4. Data were analyzed by the unpaired, two-tailed Student's t test with a Welch's correction: *p < 0.05, ** p < 0.01.

Supplemental Data

Contents

Supplemental Methods.....	2
Supplemental Figures.....	12
Supplemental Tables.....	25

Supplemental Materials and Methods

Reagents and General Procedures

All chemicals, unless otherwise noted, were acquired from Sigma-Aldrich and used as received without further purification. All water used was ultra-pure ($>18.2 \text{ M}\Omega\text{cm}^{-1}$), and dimethylsulfoxide was of molecular biology grade ($>99.9\%$). ^{89}Zr was produced at Memorial Sloan-Kettering Cancer Center on a TR19/9 cyclotron (Ebc Industries Inc.) via the $^{89}\text{Y}(p,n)^{89}\text{Zr}$ reaction and purified to yield ^{89}Zr with a specific activity of 196-496 MBq/ μg . Activity measurements were made using a CRC-15R Dose Calibrator (Capintec). For the quantification of activity, experimental samples were counted on an Automatic Wizard γ -counter (Perkin-Helmer). The labeling of antibodies with ^{89}Zr was monitored using silica-impregnated instant thin-layer chromatography (iTLC) paper (Pall Corp.) and analyzed on an AR-2000 radio-TLC plate reader (Bioscan Inc.). All in vivo experiments were performed according to protocols approved by the Hunter College, Weill Cornell Medical College, and Memorial Sloan Kettering Institutional Animal Care and Use Committee.

Synthesis of DFO-^{nss}trastuzumab

Trastuzumab (500 μg) was dissolved in 500 μL of phosphate-buffered saline (PBS, pH 7.4), and the pH of the solution was adjusted to 8.8-9.0 with Na_2CO_3 (0.1 M). To this solution was added 8.4 μL of DFO-NCS (5 equiv., 2 mmol/mL in DMSO) in small aliquots while gently shaking. The resulting solution was incubated at 37°C for 1 hour. The modified antibody was then purified via size exclusion chromatography (Sephadex G-25 M, PD-10 column, GE Healthcare) and concentrated using centrifugal filter units with a 50,000 Da molecular weight cut off (AmiconTM Ultra 2 mL Centrifugal Filtration Units, Millipore Corp., Billerica, MA) and phosphate buffered saline (PBS, pH 7.4)

Synthesis of DFO-^{nss}trastuzumab-PNGaseF

The deglycosylation of DFO-^{nss}trastuzumab (445 μg , 32 μL) was performed by adding 1.1 units of recombinant PNGaseF enzyme (New England BioLabs, Ipswich, MA) per 1 μg of mAb (2.2 μL , 225 U/ μL), 25 μL 500 mM sodium phosphate, pH 7.5 (G7 reaction buffer from New England Biolabs) and water to make a total volume reaction of 250 μL . The reaction was incubated at 37°C for 2 h and then purified using magnetic chitin beads (New England Biolabs)

that bind to the chitin-binding domains fused to the PNGaseF and thus facilitate separation using a magnetic purification system. Including the purification step, DFO-^{nss}trastuzumab-PNGaseF was obtained in an overall yield 75% relative to the trastuzumab starting material.

Synthesis of DFO-^{nss}trastuzumab-EndoS

The deglycosylation of DFO-^{nss}trastuzumab (445 µg, 32 µL) was performed by adding 2.0 unit of recombinant EndoS enzyme (New England BioLabs, Ipswich, MA) per 1 mg of mAb (4.5 µL, 200 U/µL), 25 µL 500 mM sodium phosphate, pH 7.5 (Glycobuffer 1 from New England Biolabs) and water to make a total volume reaction of 250 µL. The reaction was incubated at 37 °C for 2 h and then purified using magnetic chitin beads (New England Biolabs) that bind to the chitin-binding domains fused to the EndoS and thus facilitate separation using a magnetic purification system. Including the purification step, DFO-^{nss}trastuzumab-EndoS was obtained in an overall yield 74% relative to the trastuzumab starting material.

Synthesis of DFO-^{ss}trastuzumab-EndoS

Glycans Modification: The deglycosylation of trastuzumab (2.0 mg) was performed by adding 2.0 unit of recombinant EndoS enzyme (New England BioLabs, Ipswich, MA) per 1 µg of mAb, 30 µL 500 mM sodium phosphate, pH 7.5 (Glycobuffer 1 from New England Biolabs), and water to make a total volume reaction of 300 µL. The reaction was incubated at 37 °C for 24 h and then purified using magnetic chitin beads (New England Biolabs). Then, the deglycosylated trastuzumab was buffer exchanged into pre-treatment buffer (50 mM Bis-Tris, 100 mM NaCl, pH 6.0) using a centrifugal filter (2 mL Amicon filter units, Millipore Corp., Billerica, MA). The filter was first equilibrated in 50 mM Bis-Tris, pH 6.0, and then spun for 6 minutes at 5000g. After the final spin, the mAb was isolated in 168 µL of buffer (10.6 mg/mL).

GalNAz Labeling: After the EndoS treatment, 12 µL H₂O, 2 µL 1M Tris buffer pH 7.6, 2 µL 1M MnCl₂, 4 µL UDP-GalNAz (from a stock solution at 40 mM in H₂O) and 11 µL GalT (Y289L) (stock solution at 3.5 mg/mL) were added to the reaction solution to bring the final volume up to about 200 µL. This resultant solution contained final concentrations of 3.4 mg/mL antibody, 10 mM MnCl₂, 0.8 mM UDP-GalNAz, and 0.1 mg/mL GalT (Y289L) and was incubated overnight at 30 °C.

DBCO-DFO Ligation: The solution from the GalNAz labeling step was purified via centrifugal filtration using 2 mL Amicon filter units and TBS, pH 7.4. After centrifugation, the modified Trastuzumab (1805 µg in 252 µL TBS) was combined with 96.5 µL DBCO-DFO (2 mM stock solution) to yield to a solution containing 1.2 mg/mL trastuzumab and 0.1 mM DBCO. This solution was incubated overnight at 25°C.

Purification: After DBCO-DFO labeling, the completed antibody was purified via size exclusion chromatography (PD10 column, GE Healthcare) and concentrated using centrifugal filter units with a 50,000 Da molecular weight cut off (Amicon™ Ultra 2 mL Centrifugal Filtration Units, Millipore Corp., Billerica, MA) and phosphate buffered saline (PBS, pH 7.4).

SDS-PAGE Analysis

The purified constructs — trastuzumab, DFO-^{nss}trastuzumab, DFO-^{nss}trastuzumab-PNGaseF, DFO-^{nss}trastuzumab-EndoS, and DFO-^{ss}trastuzumab-EndoS — were characterized via sodium dodecyl sulfate-polyacrylamide gel electrophoresis (SDS-PAGE). Briefly, 2 µg antibody (0.85 µL of a 5.89 mg/mL stock) were combined with 31.65 µL H₂O, 5 µL 500 mM dithiothreitol (NuPAGE® 10X Sample Reducing Agent, Life Technologies), and 12.5 µL 4X electrophoresis buffer (NuPAGE® LDS Sample Buffer, Thermo Fisher, Eugene, OR). This mixture was then denatured by heating to 95 °C for 10 min using a heat block. Subsequently, 20 µL of each sample was then loaded alongside an appropriate molecular weight maker (Mark12™ stained standard, Life Technologies) onto a 1 mm, 10 well 4-12% Bis-Tris protein gel (Life Technologies) and run for ~4 h at 10 V/cm in MOPS buffer. The completed gel was washed 3 times with H₂O, stained using SimplyBlue™ SafeStain (Life Technologies) for 1 h, and destained overnight in H₂O. The gel was then analyzed using an Odyssey Infrared Gel Scanner (Li-Cor Biosciences, Lincoln, NE).

Characterization of the Deglycosylated Trastuzumab DFO-immunoconjugates:

The efficiency of deglycosylation of DFO-trastuzumab immunoconjugates with EndoS and PNGaseF, and the homogeneity of the resulting preparations was evaluated by performing a carbohydrate analysis of these variants. Briefly, 1 µg of each of the following variants – unmodified trastuzumab, DFO-^{nss}trastuzumab, DFO-^{nss}trastuzumab-EndoS, DFO-^{ss}trastuzumab-

EndoS and DFO-^{nss}trastuzumab-PNGaseF were electrophoresed in two 4-12% Bis-Tris polyacrylamide gels under reducing conditions at 70V for 6 hrs. One of the gels was retained for staining with Coomassie blue, whilst the other was used for a Western Blot by transferring the proteins from the gel onto a 0.2 micron nitrocellulose membrane. Upon completion of the transfer, the membrane was immersed in Ponceau S stain for 1-2 minutes and immediately washed with filtered deionized water to visualize the heavy and light chain bands – indicative of their successful transfer onto the membrane. After rinsing the Ponceau S stained nitrocellulose membrane with water, it was blocked by incubation in Carbo-Free blocking solution (Vector Laboratories) for 30 minutes at room temperature. Thereafter, the membrane was incubated in phosphate-buffered saline (PBS) containing 1 µg/mL of biotinylated lectin – Lens Culinaris Agglutinin (LCA) for 30 mins with constant shaking at room temperature.

While the membrane was incubating with the biotinylated lectin, the Vectastain Elite ABC Reagent (Vector Laboratories) was prepared. Briefly, 100 µL each of reagent A and reagent B were added to 5 mL of the Carbo-free blocking solution and this mixture was allowed to stand for 30 minutes prior to use. The membrane was rinsed 3x with PBS-T (PBS containing 0.05% Tween-20) before adding the Vectastain Elite ABC Reagent to membrane allowing it to incubate submerged in this solution for 30 minutes. Next, the membrane was rinsed 3x with PBST before adding the chemiluminescent DuoLux substrate (Vector Laboratories) prepared by mixing equal volumes of reagent 1 and reagent 2. The membrane was rinsed 3x for 5 minutes each with PBS before draining off any excess buffer onto a blotting paper. Thereafter, the chemiluminescent substrate was added to the blot and allowed to incubate for 5 minutes at room temperature with constant shaking to insure uniform spread of the substrate over the membrane. Finally, the membrane was rinsed 3x with PBS and excess buffer was drained off prior to exposure of the blot against an X-ray film followed by development of the film in the dark room.

The rationale for using lens culinaris agglutinin (LCA) is based on its ability to bind to α -linked mannose residues. Indeed, such mannose residues are present in the biantennary heptasaccharide structure of the glycans linked to N297 in the Fc-portion of most immunoglobulins including trastuzumab (Fig.1). While treatment of the DFO-trastuzumab immunoconjugates with EndoS cleaves within the chitobiose core of the glycan to produce partially truncated glycan, it successfully removes the mannose residues at the fork of the biantennary structure of glycans present in immunoglobulins. Thus, deglycosylation with both EndoS and PNGaseF results in the removal of the mannose residues to which the biotinylated

form of the lectin can bind to yield a signal on an LCA blot. This is evidenced by the fact that only unmodified native trastuzumab and DFO-^{nss}trastuzumab yielded a signal on the LCA blot shown in *Figure S3* despite a long exposure – indicating successful and quantitative deglycosylation of DFO-trastuzumab immunoconjugates achieved by the two enzymes – EndoS and PNGaseF.

In Vitro FcγRI Binding ELISA

Recombinant mouse or human Fc gamma RI/CD64, CF (R&D Systems #2074-FC-050 or #1257-FC-050) was diluted to 10 µg/ml in sterile PBS and 100 µL/well was coated overnight at 4 °C onto an ELISA plate (Plates- Nunc MaxiSorp[®] flat-bottom 96 well plate, Fisher Scientific). After a brief blocking period (40 min with PBS containing 10% FCS), the immunoconjugates were diluted in blocking buffer (0.5 or 50 µg/ml) and 100 µL/well were applied for 2 hours at room temperature. As not to disrupt the Fc-FcγRI interactions, the bound immunoconjugates were detected using 1:5000 HRP-labeled anti-human IgG (JacksonImmunoResearch Laboratories, West Grove, PA). After a final wash step, TMB substrate was used to develop the bound HRP secondary antibody, and the color reaction was stopped with 2N H₂SO₄. Optical Densities at 450 nm were determined using a SpectraMax i3 plate reader (Molecular Devices). Binding data was collected in triplicate, averaged, and plotted.

Surface Plasmon Resonance

Kinetic constants for the on-rate (k_a), off-rate (k_d) and binding affinity (K_D) of trastuzumab and its various immunoconjugates – DFO-^{nss}trastuzumab, DFO-^{nss}trastuzumab-EndoS, DFO-^{ss}trastuzumab-EndoS and DFO-^{nss}trastuzumab-PNGaseF were determined via surface plasmon resonance (SPR) on a Biacore T200 (GE Healthcare). Briefly, two types of interactions were analyzed via SPR in this study. First, we studied the impact on the immunoreactivity of the different trastuzumab variants for its cognate antigen – Her2 – with respect to the degree of deglycosylation of the antibody and the site of choice for conjugation of the radiometal chelator – DFO. Next, since deglycosylation of immunoglobulins is known to affect its binding to Fcγ receptors (FcγR) – we investigated the impact of deglycosylation and site of DFO conjugation on the binding of the various trastuzumab immunoconjugates with human as well as murine FcγR1.

For the first set of investigations, separate SPR experiments (n=3 per trastuzumab immunoconjugate) were performed using trastuzumab or its DFO-immunoconjugate variants as

the ligand captured on a Protein A sensor chip (29-1275-56, GE Healthcare). The capture of the various immunoconjugates was accomplished by diluting the IgG to a concentration of 1 µg/mL in HBS-EP+ buffer (BR100188, GE Healthcare) and injecting it over a Series S protein A sensor chip for 30 sec at a flow rate of 5 µL/min. Purified recombinant human Her2 protein (HE2-H822R Acro Biosystems) was used as the analyte and injected over the sensor chip coated with native trastuzumab or the various DFO-immunoconjugates. The binding kinetics was evaluated over a concentration series of Her2 used as the analyte (50 nM, 25 nM, 12.5 nM, 6.25 nM, 3.13 nM, 1.56 nM, 0.78 nM and 0.39 nM) re-suspended in HBS-EP+ buffer. Each concentration of the Her2 analyte was injected over the sensor chip surface for 5 minutes at a flow rate of 5 µL/min to facilitate the binding interaction with the antibody/immunoconjugate captured on the sensor chip. Next, the binding buffer (HBS-EP+) was allowed to flow over the sensor chip for 15 minutes at a flow rate of 5 µL/min to allow dissociation of Her2 from the trastuzumab-Her2 antigen immunocomplex on the chip. Finally, the regeneration buffer (10 mM Glycine-HCl pH 2.0) was passed over the chip surface for 1 min at a flow rate of 5 µL/min to achieve complete dissociation of the captured antibody and any remaining immunocomplexes. HBS-EP+ buffer was flown (5 µL/min) over the chip for 2 minutes to stabilize the protein A chip surface prior to injection of the next sample in the concentration series of the Her2 analyte used in this experiment.

Next, to investigate the impact of deglycosylation and the choice of site for DFO conjugation with trastuzumab, we investigated the interaction between the various trastuzumab immunoconjugates and the human as well as mouse analog of the high affinity Fc-receptor FcγRI. To this end, a histidine-tagged variant of recombinant human FcγRI (500238; NovoPro Labs), hereafter referred to as huFcR1, was captured as the ligand on a Series S sensor chip NTA (BR-1005-32; GE Healthcare). The NTA chip was charged with nickel ions (Ni²⁺) by performing a low sample consumption injection of 0.5 mM NiCl₂ from the NTA Reagent kit (28-9950-43; GE Healthcare) for 60 seconds at a flow rate of 10 µL/min, followed by an extra wash with HBS-P+ buffer containing 3 mM EDTA. Next, to capture the ligand, a 2nM solution of huFcR1 in running buffer (HBS-P+ buffer containing 50 µM EDTA) was injected over flow-cell 2 for 60 seconds at a flow rate of 10 µL/min. High performance injections of the various analyte concentrations of trastuzumab or its DFO-immunoconjugates (50 nM, 25 nM, 12.5 nM, 6.25 nM, 3.13 nM, 1.56 nM, and 0.78 nM) were performed over flow cells 1 and 2 for 300 seconds at a flow-rate of 30 µL/min. To shorten the length of the SPR run without compromising the analysis

of the bimolecular interaction, the dissociation of the immunoconjugate(s) from the huFcR1 captured on the NTA chip was assessed over 2 different lengths of time – 900s for the highest concentration of analyte used in the experiment (50 nM), whereas 300s for all the other concentrations of the analyte used in this experiment. Finally, the surface of the flow cells on the NTA chip was regenerated using a 60s injection of 350 mM EDTA (NTA Reagent kit) at a flow-rate of 30 μ L/min, followed by an extra wash using the running buffer. A similar experimental set up was used to evaluate the interaction between the various trastuzumab immunoconjugates and murine Fc-receptor using SPR. However, the following changes were made. First and foremost, 5 nM of a histidine-tagged variant of recombinant mouse Fc γ R1 (2074-FC; R&D Systems), hereafter referred to as muFcR1, was captured on a Series S sensor chip NTA. While everything else was kept the same as what was used for the huFcR1, the dissociation of the various immunoconjugates from the muFcR1 was evaluated over a short time window of 180s. The choice for the truncated analysis of the dissociation phase was premised on the fact that mouse Fc γ R1 has 2 binding sites for human or humanized IgG1 molecules and has been shown to display biphasic binding with these molecules. Thus, the first 3 minutes of the dissociation phase was considered suitable for the purpose of this study to compare the binding of a humanized antibody and its immunoconjugate variants with human as well as mouse analogs of Fc γ R1 using the standard 1:1 Langmuir binding to fit the data generated from the SPR analysis. The BIAcore T200 evaluation software was used to analyze the kinetic data and the 1:1 Langmuir binding fit (RI set to 0) was used to derive kinetic constants representative of the interaction between trastuzumab and its various DFO-immunoconjugates with purified Her2 protein and the human and murine analogs of Fc γ R1.

Cell Culture

Human breast cancer cell line BT474 was obtained from the American Type Culture Collection (ATCC) and maintained in Dulbecco's Modified Eagle Medium: Nutrient mixture F-12 (DMEM:F12), supplemented with 10% heat-inactivated fetal bovine serum, 2.0 mM glutamine, 100 units/mL penicillin, and 100 units/mL streptomycin in a 37°C environment containing 5% CO₂. Human histiocytic lymphoma cell line U937 was obtained from Sigma-Aldrich and maintained in RPMI 1640 medium supplemented with 10% heat-inactivated fetal bovine serum, 2.0 mM glutamine, 100 units/mL penicillin, and 100 units/mL streptomycin in a 37°C environment containing 5% CO₂. Mouse monocyte/macrophage cell line RAW264.7

BT474 was obtained from the American Type Culture Collection (ATCC) and maintained in Dulbecco's Modified Eagle Medium modified to contain 4 mM L-glutamine, 4500 mg/L glucose, 1 mM sodium pyruvate, 1500 mg/L sodium bicarbonate, and fetal bovine serum to a final concentration of 10%. Cell lines were harvested and passaged when reaching 80% of confluence using a formulation 0.25% trypsin/0.53 mM EDTA in Hank's Buffered Salt Solution without calcium and magnesium.

Flow Cytometry

Flow cytometry experiments were performed with HER2-positive BT474 cells, human (U937), and mouse macrophages (RAW264.7). The RAW264.7 cells were induced just before confluence with murine interferon- γ (IFN- γ ; 200U/mL; Prepotech) in DMEM with 10% FBS and cultured for 3 days. The differentiation of human monocytes U937 into macrophages was induced by exposing the cells (5×10^5 cells/ml) to 5 ng/mL of phorbol 12-myristate 13-acetate (PMA) (Sigma) and 200 U/mL of human recombinant interferon- γ (IFN- γ) for 48 h. Native trastuzumab and the immunoconjugates were incubated at 6 μ g/ml in suspension with 10^6 cells/ml for 30 min on ice. Cells were washed by pelleting and resuspension and then incubated with a goat anti-human IgG-AlexaFluor568 secondary antibody (Thermo Fisher Scientific) at 4 μ g/ml. Subsequently, the cells were again washed by pelleting and resuspension three times and then analyzed on a BD LSR-II (BD Biosciences). Binding data was collected in triplicate, averaged, and plotted.

Radiolabeling with ^{89}Zr

For each antibody construct, 400 μ g of immunoconjugate solution was diluted in 400 μ L PBS, pH 7.4. [^{89}Zr]Zr-oxalate (1300 μ Ci) in 100 μ L of 1.0 M oxalic acid was adjusted to pH 7.0-7.5 with 1.0 M Na_2CO_3 . After the bubbling of CO_2 stopped, the ^{89}Zr solution was added to the antibody solution, and the resulting mixture was incubated at room temperature for 1 h. The reaction progress was then assayed using iTLC using an eluent of 50 mM EDTA (pH 5). Subsequently, the reaction was quenched with 10 μ L of 50mM of EDTA (pH = 5), and the antibody construct was purified using size exclusion chromatography (Sephadex G-25 M, PD-10 column, GE Healthcare; dead volume = 2.5 mL, eluted with 500 μ L fractions of PBS, pH 7.4) and if necessary concentrated via centrifugal filtration units with a 50,000 Da molecular weight cut off (AmiconTM Ultra 4 Centrifugal Filtration Units, Millipore Corp. Billerica, MA). The

radiochemical purity of the final radiolabeled bioconjugate was assayed by iTLC using 50 mM EDTA (pH 5) as an eluent. In the iTLC experiments, free $^{89}\text{Zr}^{4+}$ cations and [^{89}Zr]-EDTA elute with the solvent front, while the radioimmunoconjugate remains at the baseline.

Radiolabeled Antibody Stability Assays

The stability of the radioimmunoconjugates with respect to radiochemical purity and loss of radioactivity from the antibody was investigated via incubation of the antibodies in human serum for 7 days at 37°C (n = 3). At predetermined time intervals, the radiochemical purity of the radioimmunoconjugates was determined via iTLC with an eluent of 50 mM EDTA pH 5.0.

Xenograft Models

All experiments were performed under Institutional Animal Care and Use Committee-approved protocols, and the experiments followed institutional guidelines for the proper and humane use of animals in research. Six to eight week-old athymic nude female mice were obtained from Charles River Laboratories (Wilmington, MA). Six to eight week-old NSG female and twenty week-old humanized NSG mice were obtained from Jackson Laboratories (Bar Harbor, ME). Animals were housed in ventilated cages, were given food and water ad libitum, and were allowed to acclimatize for approximately 1 week before subcutaneous implantation of an oestrogen pellet (17 β -estradiol 0.72 mg/pellet, 60-day release, from Innovative Research of America, Sarasota, FL). 5 days after the pellet implantation, BT474 tumors were induced on the left shoulder by a subcutaneous injection of 10^7 cells in a 150 μL cell suspension of a 1:1 mixture of fresh media: BD Matrigel (BD Biosciences, Bedford, MA). The xenografts reached the size of $\sim 100 \text{ mm}^3$ in approximately 25-30 days.

Acute Biodistribution

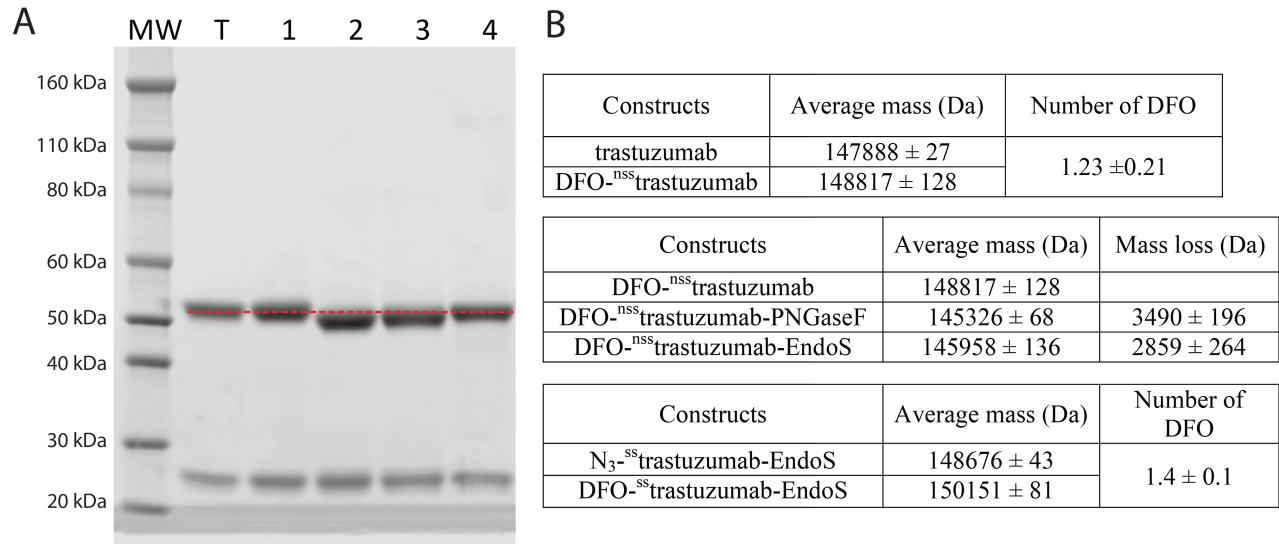
Mice (athymic nude, NSG, or humanized NSG mice) bearing subcutaneous BT474 xenografts (left shoulder; 60-120 mm^3) were randomized before the study and were administrated with the radioimmunoconjugates [20 μCi (10 μg) in 200 μL of saline] via tail vein injection. Subsequently, the animals (n = 4 per group) were euthanized by $\text{CO}_2(\text{g})$ asphyxiation at 24, 48, and 120 h post-injection, and 13 tissues (including tumor) were removed, washed, dried, weighed, and counted in a gamma counter. The number of counts in each tissue was background and decayed corrected to the time of injection and converted to activity units (μCi)

using a calibration curve generated from known standards. The %ID/g for each tissue sample was then calculated by normalization to the total activity injected and the mass of each tissue.

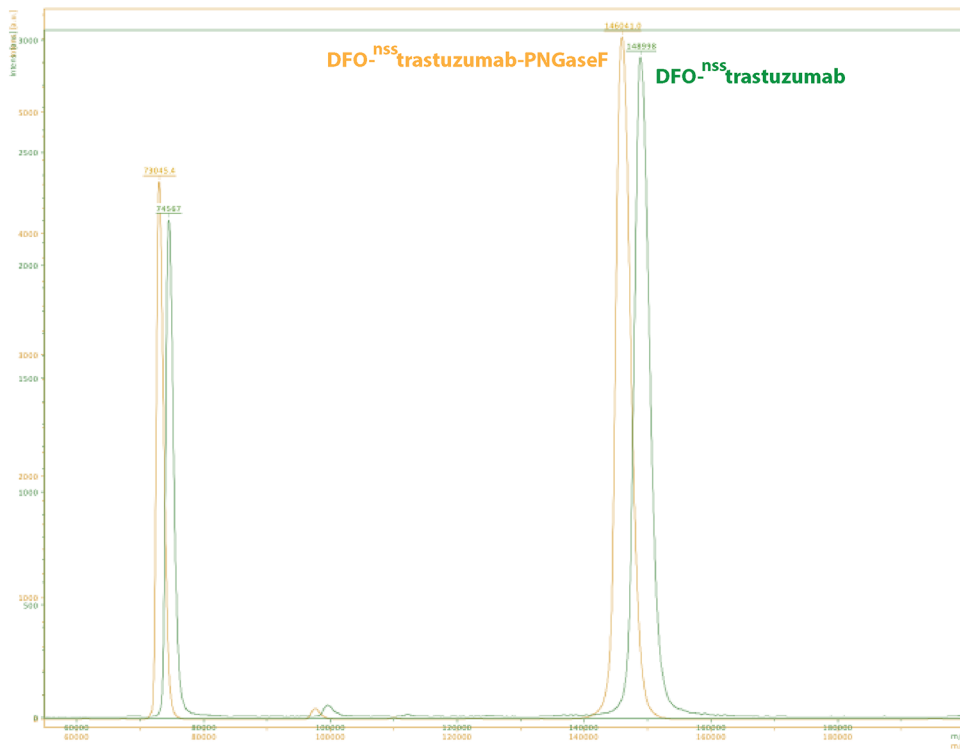
Data Availability

The datasets generated during and/or analyzed during the current study are available from the corresponding author on request.

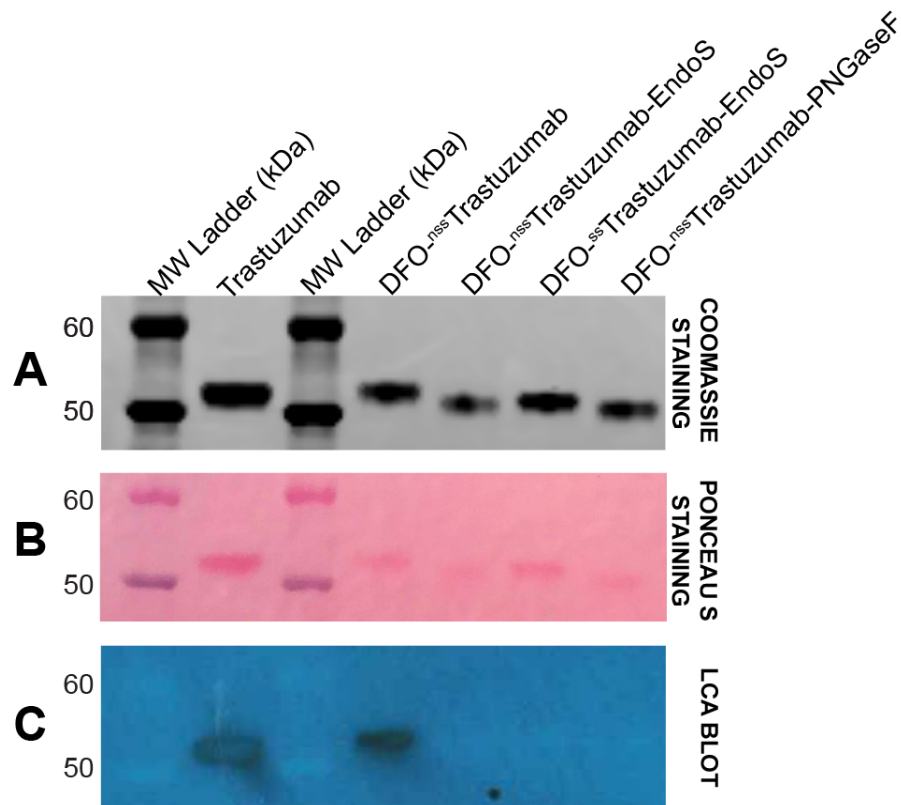
Supplemental Figures



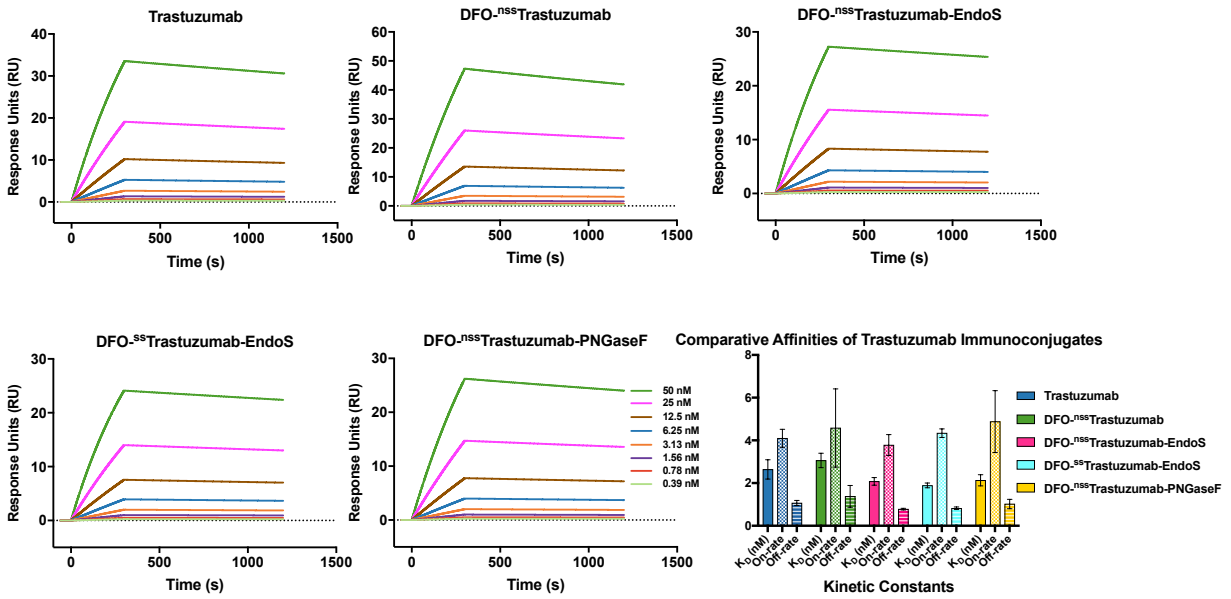
Supplemental Figure 1: Characterization of the different trastuzumab-based constructs. (a) SDS-PAGE of unmodified trastuzumab (T), DFO-^{nss}trastuzumab (1), DFO-^{nss}trastuzumab-PNGaseF (2), DFO-^{nss}trastuzumab-EndoS (3), and DFO-^{ss}trastuzumab-EndoS (4). (b) MALDI/TOF results for all immunoconjugates.



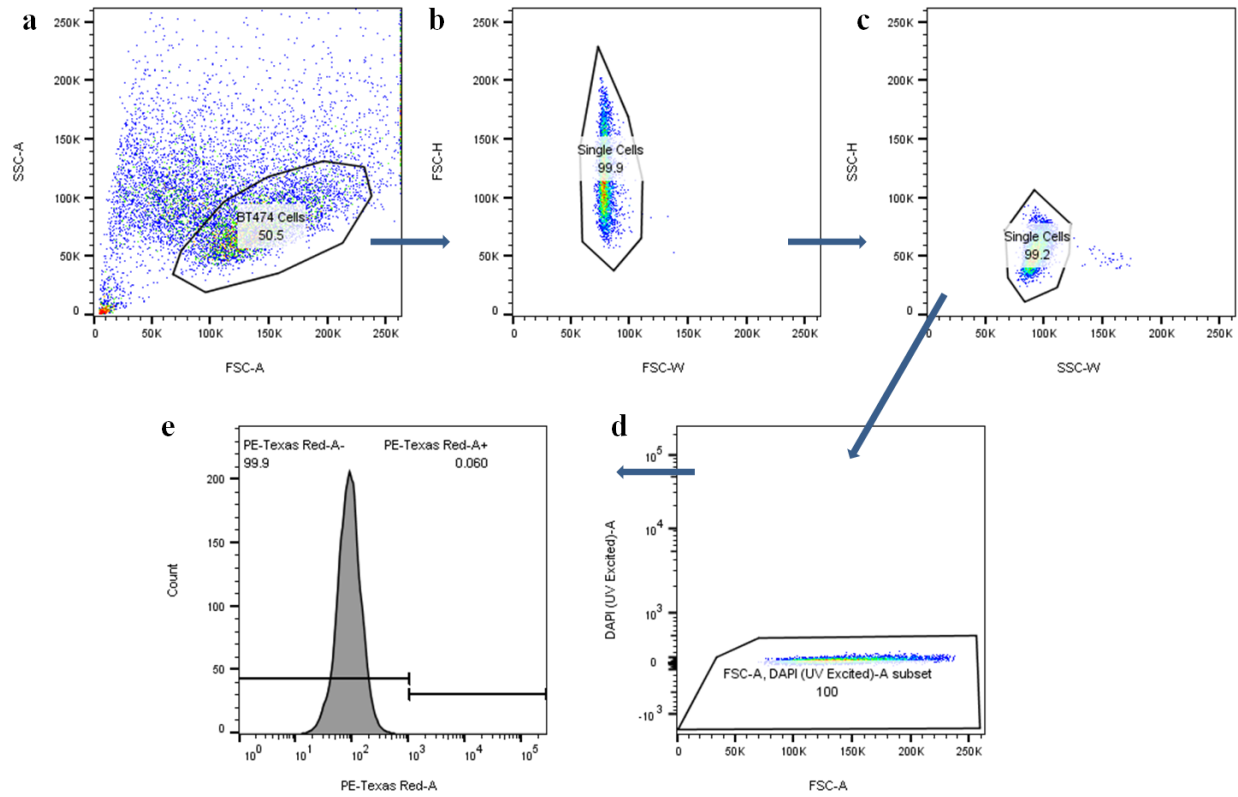
Supplemental Figure 2: Representative MALDI-ToF characterization. DFO-^{nss}trastuzumab and DFO-^{nss}trastuzumab-PNGaseF clearly create single peaks, illustrating the complete deglycosylation of the former to create the latter.



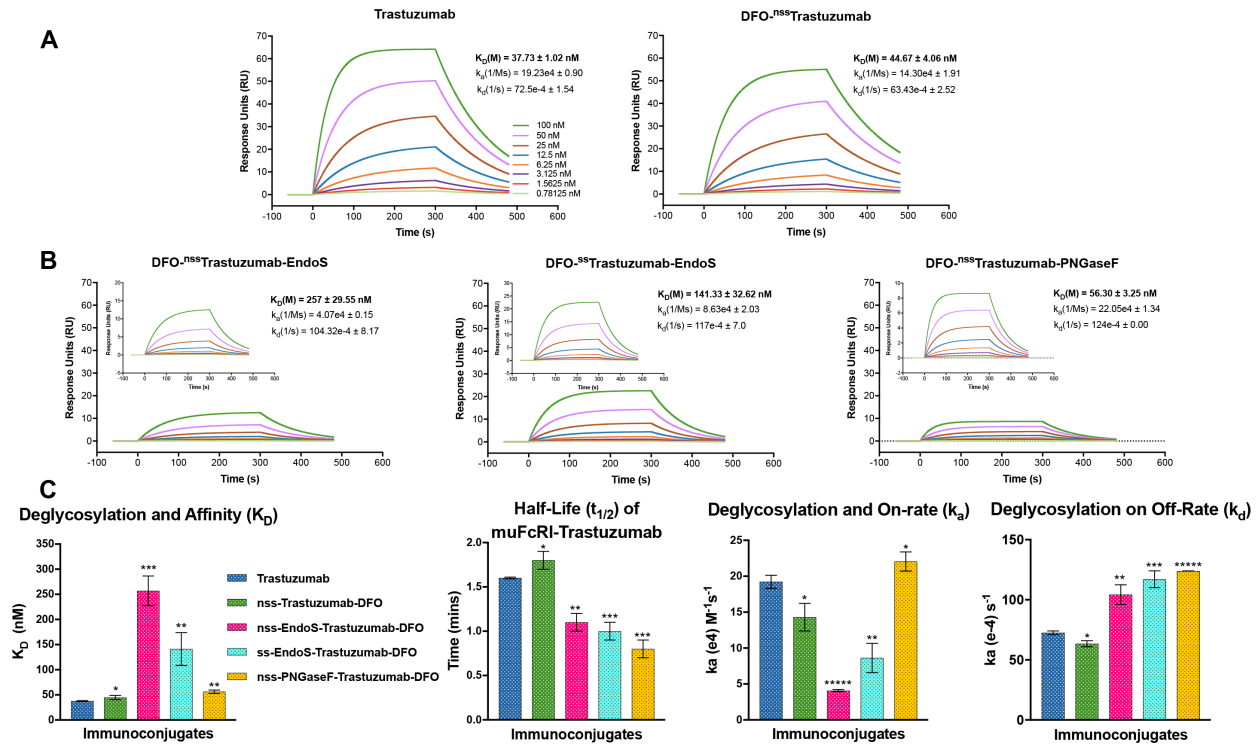
Supplemental Figure 3: The quantitative deglycosylation of DFO-bearing trastuzumab immunoconjugates is achieved with EndoS and PNGaseF. (A) Gel electrophoresis of trastuzumab and the various DFO-immunoconjugates showing a progressive downward shift in the mobility of the immunoglobulin heavy chains as a result of chemoenzymatic deglycosylation. Partial truncation of the glycan chain linked to the asparagine residue at position 297 in the Fc-portion of trastuzumab was obtained with EndoS, whereas complete truncation of the glycan chain was obtained using PNGaseF – indicated by the maximum downward shift observed in the mobility of the heavy chain for this variant; (B) Ponceau S-stained nitrocellulose membrane showing successful transfer of the immunoglobulin heavy chains from the gel; (C) Lens Culinaris Agglutinin (LCA) blot showing truncation of the glycans indicated by the absence of signal on the heavy chains of the EndoS- and PNGaseF-treated DFO-trastuzumab immunoconjugates.



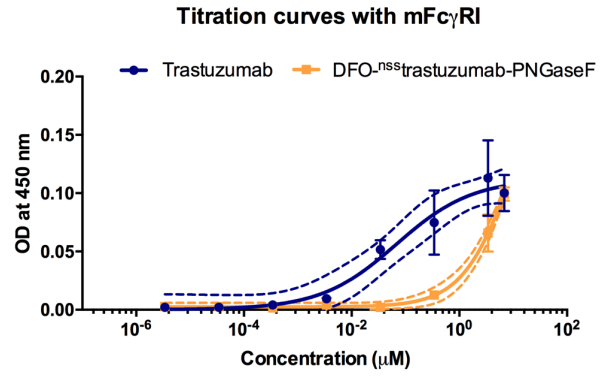
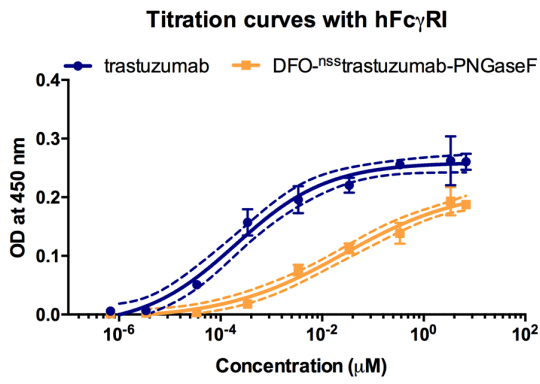
Supplemental Figure 4: Surface plasmon resonance analyses of trastuzumab and the various immunoconjugates showing comparable immunoreactivity for Her2. Sensorgrams for all the trastuzumab immunoconjugates tested in this study yielded robust concentration-dependent curves for binding kinetics to study the interaction with Her2. Unmodified trastuzumab and its various DFO-immunoconjugate variants displayed similar low nanomolar affinity constant (K_D) between 2-3 nM; a fast on-rate (k_a) between $3\text{-}5 \times 10^4 \text{ M}^{-1}\text{s}^{-1}$; and a slow off-rate (k_d) between $0.8\text{-}1.8 \times 10^{-4} \text{ s}^{-1}$.



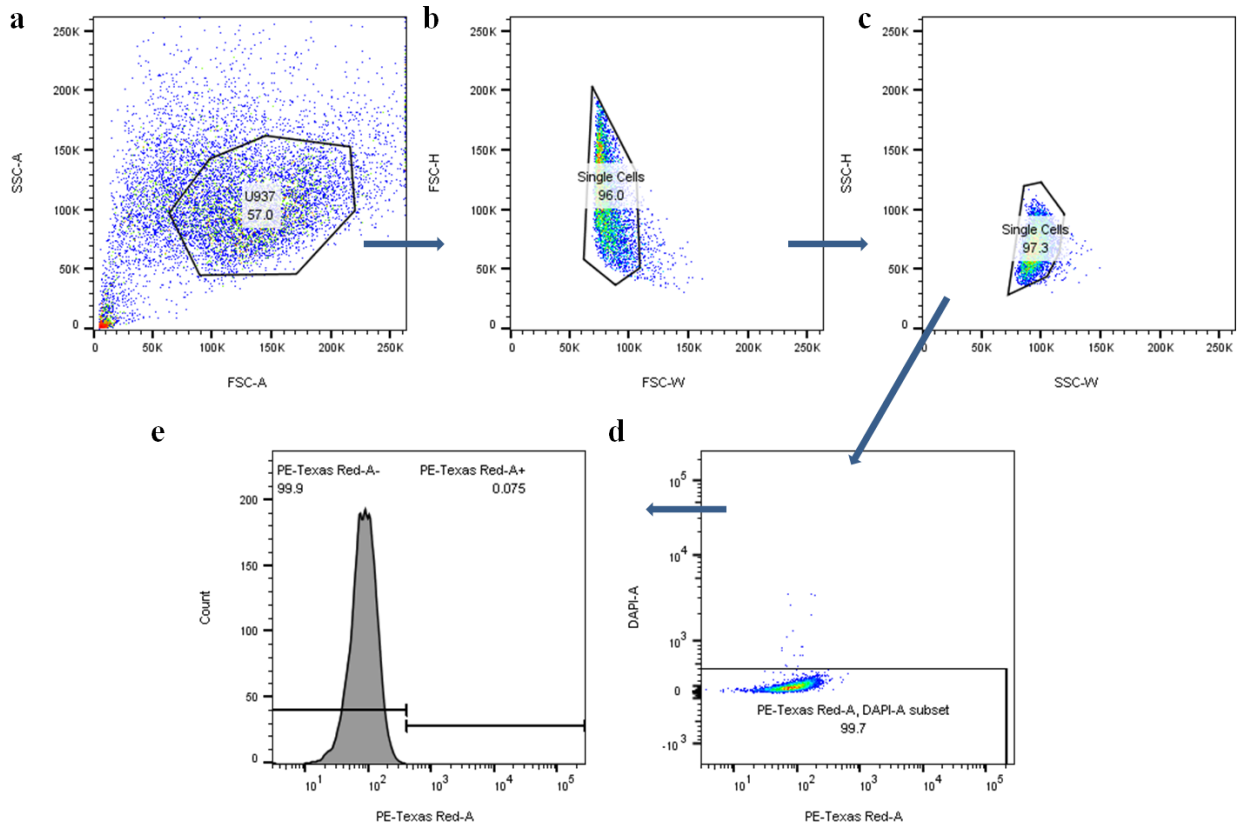
Supplemental Figure 5: Flow cytometry gating pathway for BT474 cells. (A) Initial gating was on BT474 cells as approximated by scatter, then doublets (B,C) and dead cells (D) were eliminated. (E) The limit between negative and positive cells, using unstained BT474 cells. FSC indicates forward scatter; SSC, side scatter.



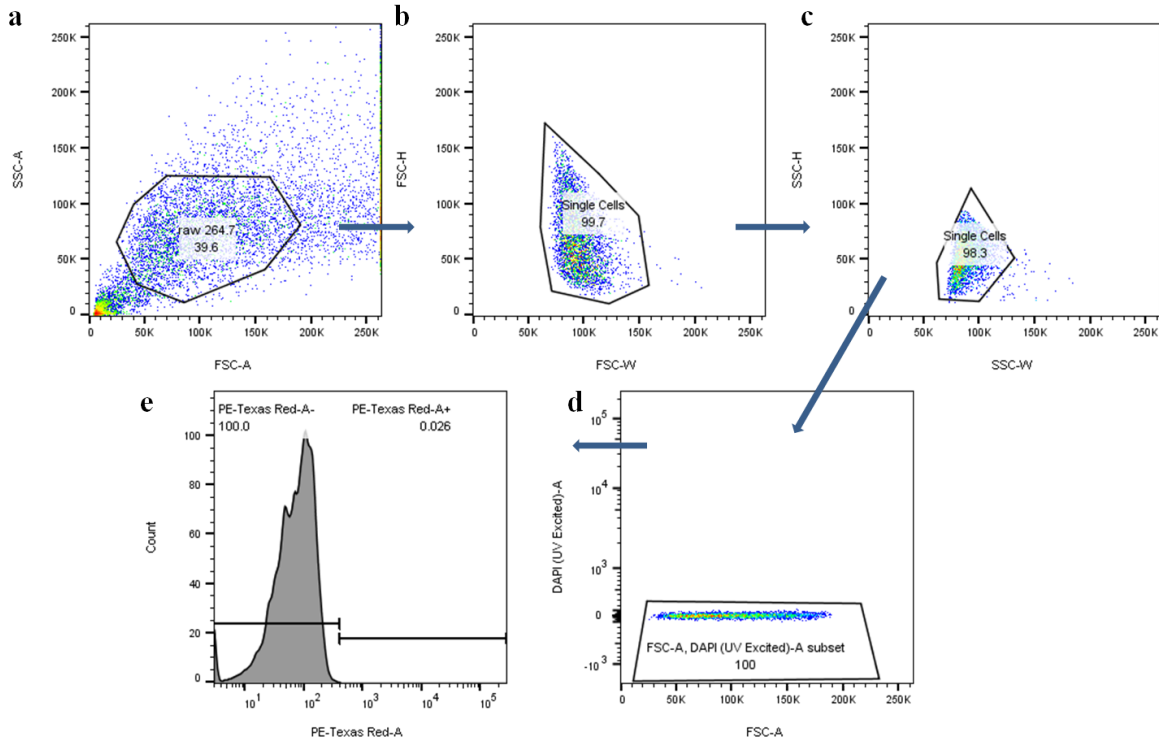
Supplemental Figure 6: Comparative SPR analysis of the interaction between trastuzumab immunoconjugates and recombinant mouse Fc γ R1. Sensorgrams showing robust concentration-dependent kinetic curves for the binding of trastuzumab and its various immunoconjugates that were used as the analyte for SPR analysis. The binding affinity and kinetic rate constants for each immunoconjugate are mentioned in the corresponding sensorgram plots shown for (A) native unmodified trastuzumab and non-site-specifically conjugated DFO-trastuzumab; and (B) deglycosylated antibody variants including Endo-S-treated, partially-deglycosylated non-site-specifically as well as site-specifically conjugated DFO-trastuzumab, and PNGaseF-treated, fully-deglycosylated non-site-specifically conjugated DFO-trastuzumab; The insets show a magnified images of the sensorgram for better visualization and appreciation of the concentration-dependent binding curves and rapid off-rates; (C) Bar graphs (left to right) showing the correlation between deglycosylation and binding affinity (K_D), half-life ($t_{1/2}$), on-rate (k_a) and off-rate (k_d). The binding affinity, half-lives and kinetic constants for each of the DFO-trastuzumab immunoconjugates were compared with those obtained for native unmodified trastuzumab. Statistically significant relationships are indicated with asterisks. * = $p < 0.05$, ** = $p < 0.005$, *** = $p < 0.0005$, **** = $p < 0.00005$.



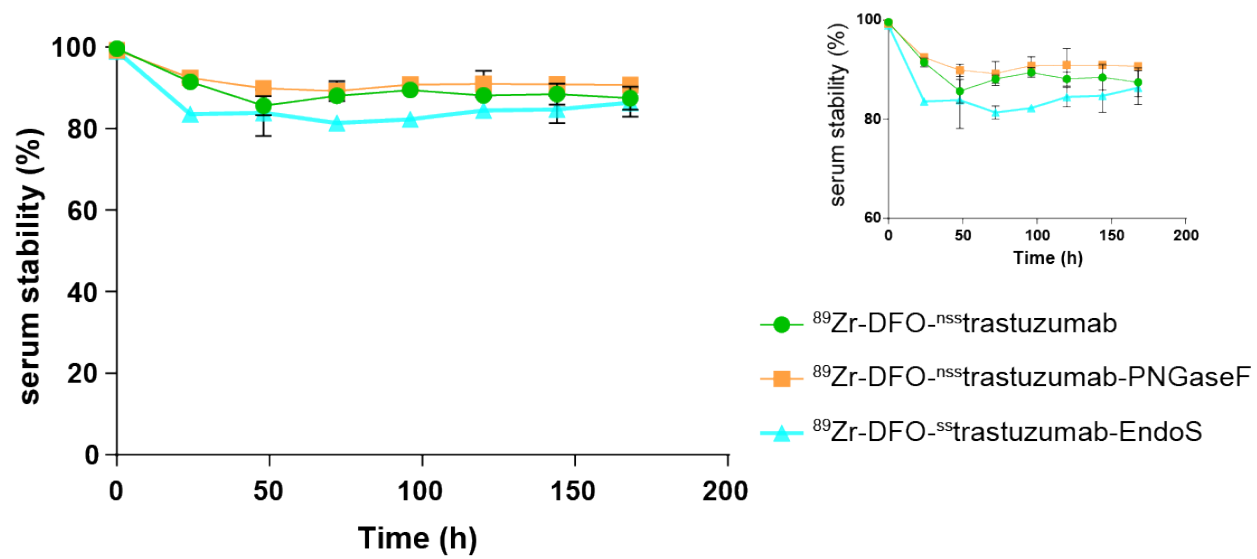
Supplemental Figure 7: ELISA titration curves of native trastuzumab and DFO-^{nss+}trastuzumab-PNGaseF with human ($p < 0.01$) and murine ($p < 0.05$) Fc γ RI.



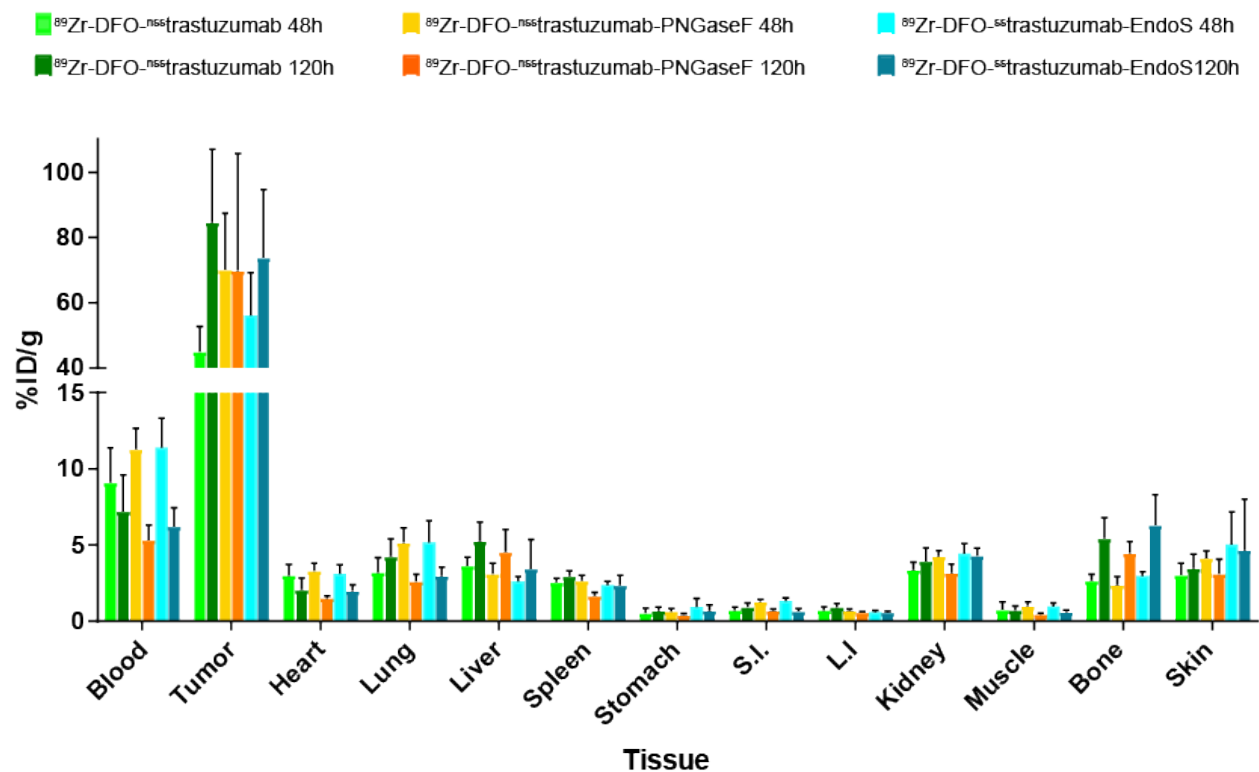
Supplemental Figure 8: Flow cytometry gating pathway for U937 cells. (A) Initial gating was on U937 cells as approximated by scatter, then doublets (B,C) and dead cells (D) were eliminated. (E) The limit between negative and positive cells, using unstained U937 cells. FSC indicates forward scatter; SSC, side scatter.



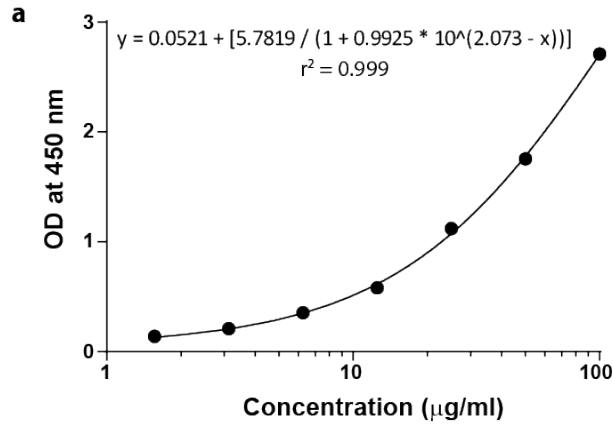
Supplemental Figure 9: Flow cytometry gating pathway for RAW 264.7 cells. (A) Initial gating was on RAW264.7 cells as approximated by scatter, then doublets (B,C) and dead cells (D) were eliminated. (E) The limit between negative and positive cells, using unstained RAW264.7 cells. FSC indicates forward scatter; SSC, side scatter.



Supplemental Figure 10: Stability of the three radioimmunoconjugates in human serum at 37 °C. Measurements were performed in triplicate (distinct samples).



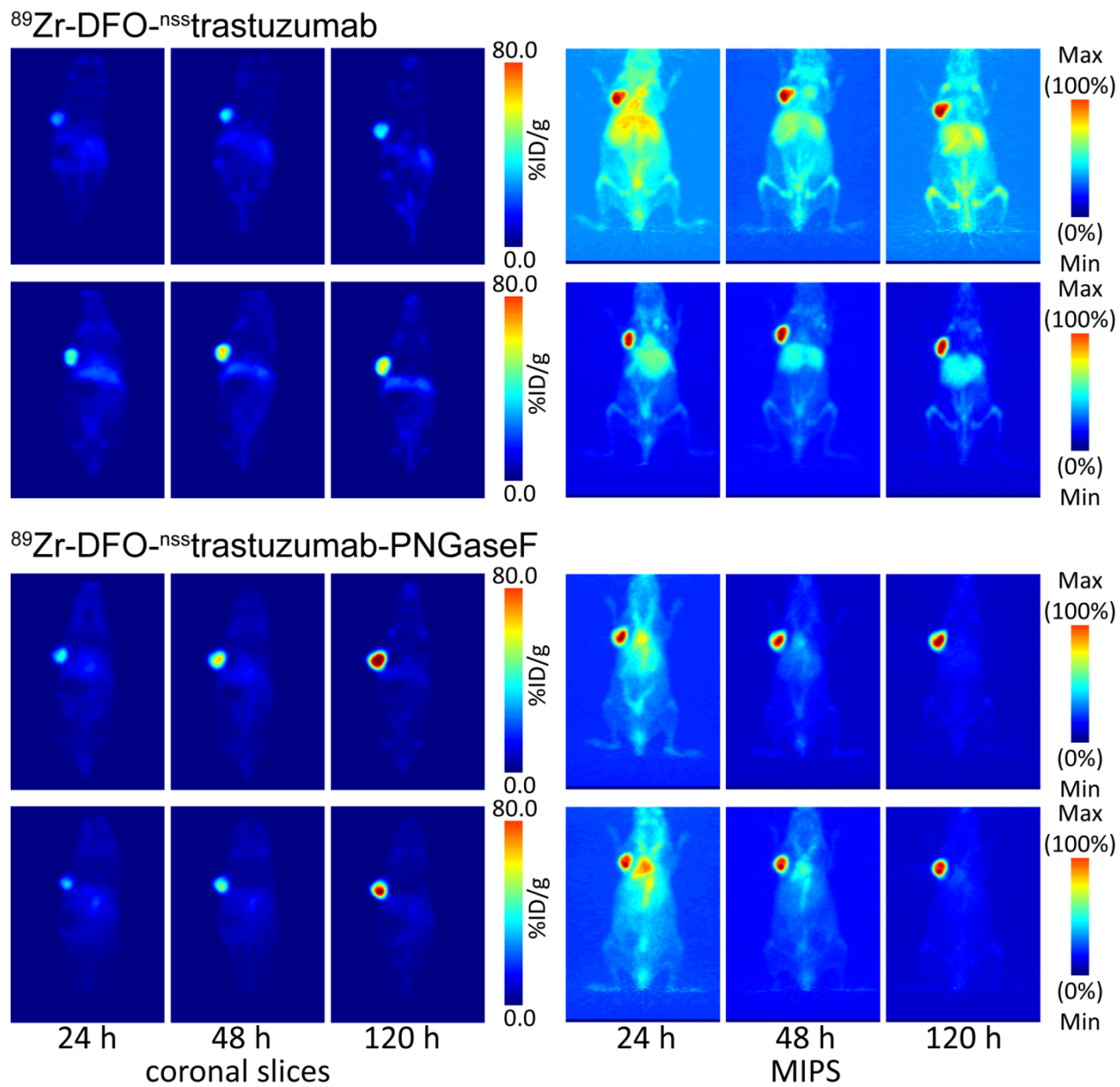
Supplemental Figure 11: Biodistribution data for $^{89}\text{Zr-DFO-nss}$ trastuzumab, $^{89}\text{Zr-DFO-nss}$ trastuzumab-PNGaseF and $^{89}\text{Zr-DFO-nss}$ trastuzumab-EndoS 48 and 120 h post-injection in nude mice bearing BT474 tumors. The values are mean \pm SD, n = 4 mice for each time point and each construct.



b

	OD at 450 nm	Concentration ($\mu\text{g/mL}$)
serum 1	0.308	109
serum 2	0.691	292
serum 3	0.564	228
serum 4	0.465	181
	Average concentration	202 \pm 67

Supplemental Figure 12: Titration of hIgG in humanized NSG mouse serum. (A) Titration curve; (B) Concentration of hIgG in different aliquots of sera.



Supplemental Figure 13: Planar (left) and maximum intensity projection (MIP, right) PET images of humanized NSG mice bearing subcutaneous BT474 xenograft between 24 h and 120 h post-injection. Each row represents the images for a single mouse.

Supplemental Tables

Immunoconjugate	k_a (1/Ms)	k_d (1/s)	K_D (M)
trastuzumab	$4.10 \pm 0.42 \times 10^4$	$1.07 \pm 0.12 \times 10^{-4}$	$2.64 \pm 0.45 \times 10^{-9}$
DFO-^{nss}trastuzumab	$4.58 \pm 1.83 \times 10^4$	$1.38 \pm 0.51 \times 10^{-4}$	$3.06 \pm 0.34 \times 10^{-9}$
DFO-^{nss}trastuzumab-EndoS	$3.78 \pm 0.49 \times 10^4$	$0.78 \pm 0.04 \times 10^{-4}$	$2.08 \pm 0.18 \times 10^{-9}$
DFO-^{ss}trastuzumab-EndoS	$4.34 \pm 0.20 \times 10^4$	$0.82 \pm 0.06 \times 10^{-4}$	$1.89 \pm 0.11 \times 10^{-9}$
DFO-^{nss}trastuzumab-PNGaseF	$4.88 \pm 1.45 \times 10^4$	$1.02 \pm 0.22 \times 10^{-4}$	$2.13 \pm 0.26 \times 10^{-9}$

Supplemental Table 1: Kinetic constants derived from SPR analysis of the interaction between trastuzumab and its various DFO-immunoconjugates with recombinant Her2.

Immunoconjugate	k_a (1/Ms)	k_d (1/s)	K_D (M)
trastuzumab	$4.91 \pm 0.18 \times 10^4$	$1.67 \pm 0.27 \times 10^{-4}$	$3.40 \pm 0.60 \times 10^{-9}$
DFO-^{nss}trastuzumab	$4.08 \pm 0.17 \times 10^4$	$1.35 \pm 0.16 \times 10^{-4}$	$3.33 \pm 0.54 \times 10^{-9}$
DFO-^{nss}trastuzumab-EndoS	$3.06 \pm 0.37 \times 10^4$	$4.91 \pm 0.21 \times 10^{-4}$	$16.27 \pm 2.72 \times 10^{-9}$
DFO-^{ss}trastuzumab-EndoS	$3.36 \pm 0.24 \times 10^4$	$7.52 \pm 0.25 \times 10^{-4}$	$22.43 \pm 2.12 \times 10^{-9}$
DFO-^{nss}trastuzumab-PNGaseF	$3.56 \pm 0.25 \times 10^4$	$21.37 \pm 0.68 \times 10^{-4}$	$60.0 \pm 2.43 \times 10^{-9}$

Supplemental Table 2: Kinetic constants derived from SPR analysis of the interaction between trastuzumab and its various DFO-immunoconjugates with recombinant huFcR1

Immunoconjugate	Half-life ($t_{1/2}$)
trastuzumab	70.5 ± 11.1
DFO-^{nss}trastuzumab	86.1 ± 9.6
DFO-^{nss}trastuzumab-EndoS	23.6 ± 1.0
DFO-^{ss}trastuzumab-EndoS	15.4 ± 0.5
DFO-^{nss}trastuzumab-PNGaseF	5.4 ± 0.2

Supplemental Table 3: Half-lives derived from SPR analysis of the interaction between trastuzumab and its various DFO-immunoconjugates with recombinant huFcR1.

Immunoconjugate	k_a (1/Ms)	k_d (1/s)	K_D (M)
trastuzumab	19.23 ± 0.90 x10 ⁴	72.50 ± 1.54 x10 ⁻⁴	37.73± 1.02 x10 ⁻⁹
DFO-^{nss}trastuzumab	14.30 ± 1.91 x10 ⁴	63.43 ± 2.52 x10 ⁻⁴	44.67 ± 4.06 x10 ⁻⁹
DFO-^{nss}trastuzumab-EndoS	4.07 ± 0.15 x10 ⁴	104.32 ± 8.17 x10 ⁻⁴	257 ± 29.55 x10 ⁻⁹
DFO-^{ss}trastuzumab-EndoS	8.63 ± 2.03 x10 ⁴	117 ± 7.0 x10 ⁻⁴	141.33 ± 32.62 x10 ⁻⁹
DFO-^{nss}trastuzumab-PNGaseF	22.05 ± 1.34 x10 ⁴	123.95 ± 0.07 x10 ⁻⁴	56.30 ± 3.25 x10 ⁻⁹

Supplemental Table 4: Kinetic constants derived from SPR analysis of the interaction between trastuzumab and its various DFO-immunoconjugates with recombinant muFcR1.

Immunoconjugate	Half-life (t_{1/2})
trastuzumab	1.6 ± 0.01
DFO-^{nss}trastuzumab	1.8 ± 0.1
DFO-^{nss}trastuzumab-EndoS	1.1 ± 0.1
DFO-^{ss}trastuzumab-EndoS	1.0 ± 0.1
DFO-^{nss}trastuzumab-PNGaseF	0.8 ± 0.1

Supplemental Table 5: Half-lives derived from SPR analysis of the interaction between trastuzumab and its various DFO-immunoconjugates with recombinant muFcR1.

	⁸⁹ Zr-DFO- ^{nss} trastuzumab		⁸⁹ Zr-DFO- ^{nss} trastuzumab-PNGaseF		⁸⁹ Zr-DFO- ^{ss} trastuzumab-EndoS	
	48 h	120 h	48 h	120 h	48 h	120 h
Average						
Blood	9.1 ± 2.3	7.2 ± 2.4	11.3 ± 1.4	5.3 ± 1.0	11.4 ± 1.9	6.2 ± 1.2
Tumor	45.1 ± 7.6	84.6 ± 22.5	70.1 ± 17.4	69.9 ± 35.9	56.2 ± 13.1	73.8 ± 21.0
Heart	3.0 ± 0.7	2.1 ± 0.8	3.3 ± 0.5	1.5 ± 0.2	3.1 ± 0.6	2.0 ± 0.4
Lung	3.2 ± 1.0	4.3 ± 1.2	5.2 ± 1.0	2.6 ± 0.5	5.2 ± 1.4	3.0 ± 0.6
Liver	3.6 ± 0.6	5.3 ± 1.2	3.1 ± 0.7	4.6 ± 1.5	2.6 ± 0.3	3.4 ± 1.9
Spleen	2.6 ± 0.2	3.0 ± 0.3	2.7 ± 0.3	1.7 ± 0.2	2.4 ± 0.2	2.4 ± 0.6
Stomach	0.5 ± 0.3	0.7 ± 0.2	0.6 ± 0.2	0.4 ± 0.1	0.9 ± 0.6	0.7 ± 0.4
Small Intestine	0.7 ± 0.2	0.9 ± 0.3	1.3 ± 0.1	0.7 ± 0.1	1.3 ± 0.2	0.7 ± 0.2
Large Intestine	0.7 ± 0.2	0.9 ± 0.2	0.7 ± 0.1	0.6 ± 0.1	0.6 ± 0.1	0.6 ± 0.1
Kidney	3.4 ± 0.5	3.9 ± 0.9	4.3 ± 0.4	3.2 ± 0.6	4.4 ± 0.6	4.3 ± 0.5
Muscle	0.7 ± 0.5	0.7 ± 0.3	1.0 ± 0.3	0.4 ± 0.1	1.0 ± 0.2	0.6 ± 0.1
Bone	2.7 ± 0.4	5.5 ± 1.3	2.4 ± 0.5	4.5 ± 0.8	3.0 ± 0.3	6.3 ± 2.0
Skin	3.0 ± 0.8	3.5 ± 0.9	4.1 ± 0.5	3.1 ± 1.0	5.0 ± 2.2	4.7 ± 3.3

Supplemental Table 6: Biodistribution data for the three constructs in nude mice bearing BT474 subcutaneous xenografts. The values are %ID/g ± SD; n = 4 mice for each time point and each construct.

Average	⁸⁹ Zr-DFO- ^{nss} trastuzumab			⁸⁹ Zr-DFO- ^{nss} trastuzumab-PNGaseF			⁸⁹ Zr-DFO- ^{ss} trastuzumab-EndoS		
	24 h	48 h	120 h	24 h	48 h	120 h	24 h	48 h	120 h
Blood	1.5 ± 0.1	0.4 ± 0.1	0.1 ± 0.0	17.1 ± 1.1	14.7 ± 0.6	7.7 ± 1.8	9.3 ± 0.4	6.3 ± 1.8	2.1 ± 0.9
Tumor	27.6 ± 10.7	17.1 ± 2.4	7.9 ± 3.3	51.5 ± 9.9	76.8 ± 10.1	87.7 ± 5.9	39.8 ± 4.3	48.0 ± 13.5	53.9 ± 11.0
Heart	1.8 ± 0.3	1.3 ± 0.1	1.0 ± 0.2	4.6 ± 0.5	3.9 ± 0.4	2.5 ± 0.5	3.0 ± 0.2	2.5 ± 0.6	1.5 ± 0.4
Lung	2.3 ± 0.4	1.4 ± 0.1	0.7 ± 0.1	10.4 ± 2.8	9.7 ± 0.6	6.4 ± 1.9	6.2 ± 0.8	4.8 ± 1.2	2.5 ± 0.6
Liver	15.5 ± 1.6	16.5 ± 1.4	15.2 ± 1.2	5.0 ± 0.5	5.6 ± 0.9	5.2 ± 0.7	9 ± 1.3	12.1 ± 2.5	10.0 ± 1.0
Spleen	46.2 ± 0.5	43.8 ± 8.1	64.4 ± 24.8	7.4 ± 1.1	7.7 ± 1.0	7.1 ± 0.3	22.4 ± 4.2	30 ± 10.1	29.8 ± 4.6
Stomach	1.7 ± 0.2	1.2 ± 0.1	0.5 ± 0.2	1.1 ± 0.1	1.0 ± 0.4	0.6 ± 0.3	0.9 ± 0.1	0.6 ± 0.1	0.4 ± 0.1
Small Intestine	5.2 ± 0.8	3.2 ± 0.3	1.8 ± 0.2	2.0 ± 0.2	1.5 ± 0.2	1.0 ± 0.2	2.7 ± 0.2	1.9 ± 0.2	1.6 ± 0.2
Large Intestine	3.1 ± 0.3	2.2 ± 0.4	0.7 ± 0.1	1.6 ± 0.2	1.7 ± 0.2	1.2 ± 0.1	1.3 ± 0.2	1.0 ± 0.1	0.7 ± 0.1
Kidney	3.4 ± 0.4	2.7 ± 0.2	2.3 ± 0.2	5.9 ± 0.3	5.1 ± 0.3	4.2 ± 0.4	4.0 ± 0.4	3.6 ± 0.4	2.9 ± 0.2
Muscle	0.6 ± 0.4	0.7 ± 0.1	0.5 ± 0.1	1.2 ± 0.3	1.2 ± 0.1	0.8 ± 0.2	1.1 ± 0.2	0.9 ± 0.1	0.8 ± 0.1
Bone	10.3 ± 1.1	12.8 ± 1.8	13.5 ± 1.5	3.7 ± 0.2	4.5 ± 0.8	8.1 ± 0.6	8.3 ± 1.2	10.2 ± 1.8	14.0 ± 1.2
Skin	2.4 ± 0.9	1.3 ± 0.2	0.7 ± 0.3	4.6 ± 0.6	3.5 ± 0.2	2.4 ± 0.6	2.9 ± 1.4	2.8 ± 0.6	2.1 ± 0.7

Supplemental Table 7: Biodistribution data for the three constructs in NSG mice bearing BT474 subcutaneous xenografts. The values are %ID/g ± SD; n = 4 mice for each time point and each construct.

Tumor/Tissue	⁸⁹ Zr-DFO- ^{ns} trastuzumab			⁸⁹ Zr-DFO- ^{ns} trastuzumab-PNGaseF			⁸⁹ Zr-DFO- ^{ss} trastuzumab-EndoS		
	24 h	48 h	120 h	24 h	48 h	120 h	24 h	48 h	120 h
Tumor/Blood	18.9 ± 7.4	49 ± 14.4	112.7 ± 67.7	3.0 ± 0.6	5.2 ± 0.7	11.4 ± 2.8	4.3 ± 0.5	7.6 ± 3	25.5 ± 12.4
Tumor/Heart	15.1 ± 6.2	13.5 ± 2.4	7.9 ± 3.8	11.2 ± 2.4	19.5 ± 3.2	34.6 ± 7.8	13.4 ± 1.6	19.4 ± 7.2	36.9 ± 12.2
Tumor/Lung	12.2 ± 5.1	11.9 ± 1.8	11.8 ± 5.5	5.0 ± 1.6	7.9 ± 1.1	13.6 ± 4.0	6.4 ± 1.1	10.1 ± 3.8	22.0 ± 7.2
Tumor/Liver	1.8 ± 0.7	1.0 ± 0.2	0.5 ± 0.2	10.4 ± 2.3	13.7 ± 2.9	17.0 ± 2.5	4.4 ± 0.8	4.0 ± 1.4	5.4 ± 1.2
Tumor/Spleen	0.6 ± 0.2	0.4 ± 0.1	0.1 ± 0.1	6.9 ± 1.7	10.0 ± 1.9	12.3 ± 0.9	1.8 ± 0.4	1.6 ± 0.7	1.8 ± 0.5
Tumor/Stomach	16.6 ± 6.7	14.6 ± 2.4	17.2 ± 9.4	46.0 ± 9.3	77.6 ± 31.5	156.5 ± 87.3	43.2 ± 6.3	78.8 ± 25.7	134.8 ± 36.3
Tumor/SI	5.3 ± 2.2	5.4 ± 0.9	4.5 ± 2.0	25.9 ± 5.7	52.6 ± 8.8	90.4 ± 17.8	14.7 ± 1.9	25.4 ± 7.6	34.1 ± 8.1
Tumor/LI	9.0 ± 3.6	7.8 ± 1.9	11 ± 5.1	32.6 ± 7.2	46.0 ± 8.4	75.6 ± 9.9	31.3 ± 5.4	47.1 ± 14.6	77.0 ± 17.1
Tumor/Kidney	8.2 ± 3.4	6.3 ± 1.0	3.4 ± 1.5	8.7 ± 1.7	15.1 ± 2.2	21.0 ± 2.4	10.0 ± 1.5	13.3 ± 4.1	18.4 ± 4.0
Tumor/Muscle	43.2 ± 31.1	25.2 ± 4.4	16.8 ± 8.3	41.5 ± 13.6	63.5 ± 9.1	109.6 ± 25.7	35.2 ± 6.8	51.7 ± 15.1	71.9 ± 19.3
Tumor/Bone	2.7 ± 1.1	1.3 ± 0.3	0.6 ± 0.3	14.0 ± 2.8	17.0 ± 3.9	10.8 ± 1.0	4.8 ± 0.8	4.7 ± 1.6	3.9 ± 0.9
Tumor/Skin	11.6 ± 6.4	13.5 ± 2.7	11.1 ± 6.2	11.1 ± 2.5	21.9 ± 3.2	36.7 ± 9.8	13.6 ± 6.7	16.9 ± 6.0	25.3 ± 9.4

Supplemental Table 8: Tumor to tissue ratios for the three constructs in NSG mice bearing BT474 xenografts. The values are %ID/g ± SD; n = 4 mice for each time point and each construct.

	⁸⁹ Zr-DFO- ^{nss} trastuzumab	⁸⁹ Zr-DFO- ^{nss} trastuzumab-PNGaseF	P value
Blood	0.5 ± 0.1	10.3 ± 2.2	0.016, *
Tumor	48.4 ± 22.5	102.1 ± 18.5	0.035, *
Heart	1.5 ± 0.2	3.1 ± 0.5	0.022, *
Lung	2.1 ± 0.8	6.8 ± 0.9	0.002, **
Liver	16.3 ± 3.5	4.7 ± 1.2	0.020, *
Spleen	71.9 ± 47.9	15.0 ± 6.8	0.038, *
Stomach	1.2 ± 0.2	0.7 ± 0.3	0.067, ns
Small Intestine	4.2 ± 0.3	1.5 ± 0.2	0.001, ***
Large Intestine	2.1 ± 0.4	1.6 ± 0.2	0.183, ns
Kidney	3.8 ± 0.7	4.7 ± 0.4	0.147, ns
Muscle	0.4 ± 0.2	1.1 ± 0.1	0.022, *
Bone	11.6 ± 1.8	5.3 ± 1.4	0.011, *
Skin	3.1 ± 0.2	6.0 ± 0.9	0.022, *

Supplemental Table 9: Biodistribution data for ⁸⁹Zr-DFO-^{nss}trastuzumab and ⁸⁹Zr-DFO-^{nss}trastuzumab-PNGaseF 120 post injection in humanized NSG mice bearing BT474 subcutaneous xenograft (n = 4 for each construct). Values are %ID/g ± SD. P values were calculated with a Welch's correction t-test.